The *Leishmania donovani* chaperone cyclophilin 40 is essential for intracellular infection independent of its stage-specific phosphorylation status

Wai-Lok Yau[1,2], Pascale Pescher[1], Andrea MacDonald[2], Sonia Hem[3], Dorothea Zander[2], Silke Retzlaff[3,+], Thierry Blisnick[4], Brice Rotureau[4], Heidi Rosenqvist[5,++], Martin Wiese[5], Philippe Bastin[4], Joachim Clos[2], and Gerald F. Späth[1,*]

Institut Pasteur and Centre National de la Recherche Scientifique URA 2581, [1]Unité de Parasitologie Moléculaire et Signalisation, and [4]Unité de Biologie Cellulaire des Trypanosomes, 25 rue du Dr Roux, F-75015 Paris, France; [2]Clos Group (Leishmanasis) and [3]Electron Microscopy Service, Bernhard-Nocht-Institut für Tropenmedizin, Bernhard-Nocht-Str. 74, D-20359 Hamburg, Germany; [3]Plate-forme de spectrométrie de masse protéomique - MSPP, Biochemie et Physiologie Moléculaire des Plantes, UMR 5004 CNRS/UMR 0386 INRA/Montpellier SupArgo/Université Montpellier II, F-34060 Montpellier, France; [5]Strathclyde Institute of Pharmacy and Biomedical Sciences, University of Strathclyde, Glasgow, Scotland, UK

* Correspondence: Gerald Späth
Institut Pasteur, 25 rue du Dr Roux, 75015 Paris, France
Phone: +33.1.40.61.38.58; Fax: +33.1.45.68.83.33
E-mail: gerald.spaeth@pasteur.fr

Short title: LdCyP40 null mutant analysis

Key words: *Leishmania donovani*, stress protein, cyclophilin 40, null mutant analysis, intracellular survival, chaperone phosphorylation

+current address: Altona Diagnostics, Moerkenstr. 12, 22767 Hamburg, Germany

++current address: Novo Nordisk, Novo Nordisk Park 1, DK-2760 Maaloev, Denmark

Summary

During its life cycle, the protozoan pathogen *Leishmania donovani* is exposed to contrasting environments inside insect vector and vertebrate host, to which the parasite must adapt for extra- and intracellular survival. Combining null mutant analysis with phosphorylation site-specific mutagenesis and functional complementation we genetically tested the requirement of the *Leishmania donovani* chaperone cyclophilin 40 (LdCyP40) for infection. Targeted replacement of LdCyP40 had no effect on parasite viability, axenic amastigote differentiation, and resistance to various forms of environmental stress in culture, suggesting important functional redundancy to other parasite chaperones. However, ultra-structural analyses and video microscopy of *cyp40-/-* promastigotes uncovered important defects in cell shape, organization of the subpellicular tubulin network and motility at stationary growth phase. More importantly, *cyp40-/-* parasites were unable to establish intracellular infection in murine macrophages and were eliminated during the first 24h post infection. Surprisingly, *cyp40-/-* infectivity was restored in complemented parasites expressing a CyP40 mutant of the unique S274 phosphorylation site. Together our data reveal non-redundant CyP40 functions in parasite cytoskeletal remodeling relevant for the development of infectious parasites *in vitro* independent of its phosphorylation status, and provides a framework for the genetic analysis of *Leishmania*-specific phosphorylation sites and their role in regulating parasite protein function.

Introduction

Parasitic protozoa of the genus *Leishmania* are the etiological agents of leishmaniases, severe human diseases with clinical manifestations ranging from self-curing cutaneous lesions to fatal visceral infection. During the infectious cycle, *Leishmania* replicate as extracellular flagellated promastigotes in the midgut of female phlebotomine sand flies where they undergo an environmentally triggered differentiation process termed metacyclogenesis to develop into highly infectious metacyclic promastigotes (Sacks *et al.*, 1984). Following transmission by blood feeding sand flies, metacyclic parasites are engulfed by phagocytes such as macrophages, where they differentiate into non-motile amastigotes that cause the pathology of the disease.

In vitro differentiation of infectious metacyclic parasites is induced by nutritional starvation or acidic pH, and development of amastigote-like cells in culture is triggered by pH and temperature change (Zakai *et al.*, 1998; Cunningham *et al.*, 2001; Barak *et al.*, 2005), suggesting that *Leishmania* stage-differentiation occurs through sensing of environmental stress signals encountered inside insect and vertebrate hosts (Zilberstein *et al.*, 1994). Recently, a role of stress signaling in parasite development has been suggested based on phosphoproteomics studies. Gel-based proteomics approaches comparing enriched phosphoprotein fractions from promastigotes and axenic amastigotes revealed a surprising divergence of the stage-specific phosphoproteome with more than 30% of proteins showing statistically significant differential phosphorylation (Morales *et al.*, 2008; Morales *et al.*, 2010). Phosphorylation events in amastigotes were almost exclusively restricted to heat shock proteins and chaperones and occurred largely at parasite-specific phosphorylation sites (Hem *et al.*, 2010), suggesting regulation of the *Leishmania* response to stress by post-translational rather than classical transcriptional mechanisms. This possibility has been investigated previously for the stress-induced protein 1 (STI1), a chaperone that acts as a scaffolding protein for the assembly of foldosome complexes (Pratt and Dittmar, 1998). Null mutant analysis of STI1 in *L. donovani*

71 established the requirement of this protein for parasite survival *in vitro,* and complementation
72 analysis by plasmid shuffle identified the two phosphorylation sites S15 and S481 as essential
73 for STI1 function and parasite viability (Morales *et al*., 2010).

74 One group of stress proteins that showed increased phosphorylation in amastigotes in
75 these studies is represented by immunophilins, a protein family that includes cyclophilins
76 (CyPs) and FK506 binding proteins (FKBPs), which are characterized by a peptidyl-prolyl
77 isomerase activity required for proper protein folding (Barik, 2006). In a previous study, we
78 revealed stage-specific functions of cyclophilins using the CyP inhibitor cyclosporin A (CsA)
79 (Yau *et al.*, 2010). Inhibitor-treated promastigotes underwent non-synchronous cell cycle arrest
80 and acquired features similar to amastigotes, including oval shape and shortening of the flagella
81 reminiscent of *L. donovani* promastigotes treated with the HSP90 inhibitor Geldanamycin
82 (Wiesgigl and Clos, 2001). In contrast, treatment of axenic amastigotes resulted in parasite
83 death, a phenomenon that was abrogated by temperature shift from 37°C to 26°C. While this
84 pharmacological approach suggests potential roles of cyclophilins in parasite proliferation and
85 thermotolerance and sheds new light on the stage-specific action of CsA and its lethal effects
86 on intracellular *Leishmania* (Yau *et al.*, 2010), the pleiotropic inhibition of multiple
87 cyclophilins and the phosphatase calcineurin by CsA-CyP complexes (Chappell and Wastling,
88 1992) raise questions about the specific function of each of the 17 *Leishmania* cyclophilins.

89 The effects of CsA on *L. donovani* differentiation and thermotolerance, its binding to
90 parasite cyclophilin 40 (LdCyP40) (Yau *et al.*, 2010), and its stage-speific phosphorylation in
91 the axenic amastigotes prompted us to assess the role of this co-chaperone and its modification
92 in parasite survival and infectivity combining gene deletion, phosphoproteomics, and
93 complementation approaches. CyP40 is a highly conserved bi-functional protein that carries
94 peptidyl-prolyl isomerase (PPIase) activity and forms dynamic complexes in yeast and
95 mammalian cells with HSP90 through its conserved tetratricopeptide repeat (TPR) domains

(Hoffmann and Handschumacher, 1995). The loss-of-function study presented here identifies important roles for LdCyP40 in the development of infectious parasites *in vitro* and intracellular parasite survival independent of its phosphorylation status, thus establishing a novel link between *L. donovani* chaperone activity and stress-induced parasite differentiation relevant for host cell infection.

Results

L. donovani CyP40 is constitutively expressed but stage-specifically phosphorylated.

CyP40 belongs to the immunophilin superfamily that comprises 17 members in *Leishmania* (Yau *et al*., 2010). We first investigated the domain structure and sequence conservation of this protein across trypanosomatid parasites (*L. major*, *L. infantum*, *L. braziliensis*, *T. brucei* and *T. cruzi*) and various higher eukaryotes, including human, mouse, cow, and yeast. The putative CyP40 protein sequences were retrieved from the UniProt (http://www.uniprot.org/) and TriTrypDB databases (http://tritrypdb.org/tritrypdb/) by Blast search using *L. major* cyclophilin 40 (LmjF35.4770) as a query and aligned using ClustalW 2.0.12. *Leishmania* CyP40 displays the characteristic two-domain structure (Fig. 1A). The N-terminal cyclophilin-like domain (CLD) spans 171 residues and is highly conserved showing 68.8% of amino acid identity across the analyzed organisms. This domain carries the enzymatic peptidyl-prolyl isomerase (PPIase) function and is the target of the cyclophilin-specific inhibitor cyclosporin (CsA). The functional residues for both PPIase activity and CsA binding are highly conserved as expected from our previously published observations that *L. donovani* CyP40 carries isomerase activity and can be enriched from crude parasite extracts by affinity chromatography using immobilized CsA (Yau *et al*., 2010). In addition, a cleft localized C-terminal of the CLD domain shows a series of conserved residues that have been previously implicated in CyP40 chaperone activity (Mok *et al.*, 2006). The C-terminal part of CyP40 contains three distinct TPR motifs that are

less conserved (50.4%, 47.3% and 50.2% of identity for TPR1, 2 and 3 respectively) and together form the TPR domain known to interact with the conserved EEVD consensus sequence of HSP70 and HSP90 (Ward *et al*., 2002). Together these data identify *Leishmania* CyP40 as a highly conserved member of the eukaryote immunophilin protein family that likely interacts with HSPs and carries chaperone function.

In our previous proteomics studies on the protein phosphorylation dynamics during *Leishmania* differentiation, *L. donovani* LdCyP40 abundance was significantly increased in the phosphoproteome of axenic amastigotes when compared to promastigotes, suggesting amastigote-specific phosphorylation of this protein (Morales *et al.,* 2008; Morales *et al.,* 2010). However, this putative stage-specific phosphorylation has not been validated in *bona fide* animal-derived amastigotes, and whether the increase of abundance results from an increase in phospho-stoichiometry or simply increased protein expression has not been investigated. To distinguish between these two possibilities, we analyzed LdCyP40 stage-specific expression and phosphorylation profiles by Western blotting using total protein extracts and phosphoprotein fractions enriched by immobilized metal affinity chromatography obtained from cultured promastigotes, axenic amastigotes, and *bona fide* amastigotes purified from *L. donovani* infected hamster spleen. As judged by α-tubulin expression used as normalization control, LdCyP40 is constitutively expressed across all stages tested, but shows a significant increase in abundance in the phosphoprotein fraction of axenic and hamster-derived amastigotes (Fig. 1B) firmly establishing its stage-specific *de novo* phosphorylation and a substantial increase in the phospho-stoichiometry of this protein.

Establishment of cyp40-/- null mutants.

We established LdCyP40 null mutant parasites to study the biological functions of LdCyP40 and ultimately assess the physiological role of stage-specific CyP40 phosphorylation by

146 complementation. The endogenous alleles were replaced using two targeting constructs
147 comprising puromycin and bleomycin resistance genes flanked by the 5' and 3'UTRs of
148 LdCyP40 (Fig. 2A and Fig. S1). Respective add-back controls re-expressing LdCyP40 from the
149 ribosomal locus under the control of the CyP40 3'UTR were generated using a knock-in
150 strategy (Fig. 2A and Fig. S2). The absence of the LdCyP40 ORF and corresponding protein in
151 six independent null mutant clones and its re-expression in complemented parasites was
152 confirmed by PCR (Fig. 2B and data not shown) and Western blot analysis (Fig. 2C and Fig.
153 S3).
154
155 *Morphological characterization of cyp40-/- null mutant and add-back clones.*
156 Microscopic observation of the two independent null mutant clones *cyp40-/-* cl.4 and cl.5 and
157 four independent add-back clones as well as add-back pools derived from each null mutant
158 clone revealed important morphological alternations at stationary growth phase that correlated
159 with the absence of CyP40 expression (Fig. 3A and Fig. S4). At logarithmic growth phase,
160 CyP40 null mutant promastigotes were morphologically identical to wild-type and add-back
161 controls as judged by Giemsa staining of fixed parasite cultures (Fig. 3A, upper panels). By
162 contrast 70% of *cyp40-/-* cells at stationary growth phase of two independent null mutant clones
163 acquired a small spherical cell shape, while wild-type parasites and add-back clones showed the
164 spindle shaped cell body characteristic for stationary phase parasites (Fig. 3A, lower panels,
165 and Fig. S4). Moreover, measurements of cell body and flagellum length revealed a significant
166 reduction of the ratio between both parameters in *cyp40-/-* cells (Fig. S4B). Given the
167 reproducibility of this phenotype, most of the subsequent experiments were performed with
168 cyp40 null mutant clone 4 and its corresponding add-back pool if not otherwise stated.
169 As cell rounding is often associated with cellular stress and apoptotic cell death (Lee *et*
170 *al.*, 2002; Gannavaram and Debrabant, 2012), we next investigated integrity and ultra-structural

171 organization of CyP40 null mutant cells and controls. Wild-type, *cyp40-/-* and *cyp40-/-/+*
172 promastigotes were fixed with 2% glutaraldehyde and analyzed by scanning electron
173 microscopy (Fig. 3B). This analysis confirmed the atypical spherical cell shape of *cyp40-/-*
174 stationary phase promastigotes and provided a first indication of their cellular integrity.
175 Likewise, analysis by transmission electron microscopy revealed no overt alterations in cellular
176 organization of *cyp40-/-* cells, which showed intact nuclei and mitochondria, and absence of
177 apoptotic bodies or autophagosomes (Fig. 3C). Finally, direct assessment of cell death by
178 FACS analysis following membrane exposure of phosphatidylserine with annexin V-FITC and
179 exclusion of propidium iodide did not reveal any significant change in cell viability of
180 stationary *cyp40-/-* parasites after 6 days of *in vitro* culture (Fig. 3D). Together these results
181 rule out the possibility of cell death as the cause of *cyp40-/-* morphological alterations but
182 rather suggest a defect in parasite development and cellular remodeling at stationary phase.
183
184 *Phenotypic characterization of stationary phase cyp40-/- promastigotes.*
185 During the infectious cycle, non-infectious procyclic promastigotes differentiate into highly
186 infective metacyclic promastigotes in response to nutritional starvation after digestion and
187 excretion of the blood meal. This process is mimicked in culture during stationary growth
188 phase (Sacks *et al.*, 1984; da Silvaand Sacks, 1987) and is accompanied by the expression of
189 characteristic biological and morphological markers, including expression of high molecular
190 weight LPG and increase in SHERP mRNA abundance. The altered morphology of *cyp40-/-*
191 parasites primed us to investigate the status of these phenotypic markers. First, monitoring cell
192 density of WT, *cyp40-/-* and add-back promastigotes with a CASY cell counter, deletion of
193 CyP40 did not affect the rate of proliferation nor the density reached at stationary phase (Fig.
194 4A). Surprisingly, despite defects in stationary phase morphology, *cyp40-/-* promastigotes
195 showed normal expression of higher molecular weight LPG characteristic for stationary phase

196 parasites as revealed by Western blot analysis using the anti-LPG antibody CA7AE (Fig. 4B),
197 and induced SHERP mRNA to levels corresponding to WT and add-back controls (Fig. 4C).
198 Together these data demonstrate that *L. donovani* CyP40 is dispensable for parasite survival *in*
199 *vitro* under standard culture conditions, and is not required for metacyclic-specific glycolipid
200 remodeling or gene regulation, at least for the markers investigated here. To further
201 characterize the stationary phase defect of *cyp40-/-* parasites, we investigated the functional
202 properties of infectious, stationary phase parasites, including cell motility and intracellular
203 survival.
204
205 *CyP40 null mutants show reduced motility and a loosened sub-pellicular tubulin network.*
206 An important functional characteristic of stationary phase parasites is a significant increase in
207 motility, which is of physiological relevance in the natural setting for migration of metacyclic
208 parasites from sand fly midgut to larynx (Walters *et al*., 1989; Walters *et al*., 1993), or the
209 establishment of host cell infection (Uezato *et al*., 2005; Forestier *et al.*, 2011). We quantified
210 motility in at least 741 WT, *cyp40-/-* and add-back promastigotes obtained from logarithmic
211 and stationary phase cultures utilizing video microscopy and *in silico* tracking analysis.
212 Qualitative observation of each movie did not reveal any significant difference in flagellar
213 wave orientation and flagellar beating amplitude across all lines and both culture conditions
214 (data not shown). Likewise, quantitative analysis showed no significant difference in beating
215 frequencies and speed between WT, *cyp40-/-*, and add-back log phase promastigotes. As
216 expected, WT and add-back promastigotes showed a statistically significant increase in motility
217 speed and flagellar beat frequency at stationary phase (Fig. 5A), and moved in a uni-directional
218 way over extended distances (Fig. 5B and Video S1). By contrast, CyP40 null mutant parasites
219 do not increase speed at stationary growth phase (Fig. 5A) and show a defect in directional
220 motility as they largely spin on themselves (Fig. 5B and Video S1).

As judged by transmission electron microscopy, this motility defect was not caused by alterations in flagellar structure of *cyp40-/-* parasites, which maintained the characteristic 9+2 organization of the axoneme (Fig. 5C). However, investigating more closely the *Leishmania* sub-pellicular tubulin network by scanning EM after removal of the parasite plasma membrane by detergent treatment, stationary phase *cyp40-/-* promastigotes showed a significantly loosened tubulin network, in contrast to the very dense, small-meshed network observed in wild-type parasites (Fig. 5D). Western blot analysis of WT, *cyp40-/-* and add-back parasites from log and stationary cultures did not reveal any significant difference in expression levels of α- and β-tubulin, with the exception of a small β-tubulin isoform at around 33kDa, which is specific for stationary phase cells and slightly reduced in CyP40 null mutants (Fig. 5E). These data demonstrate non-redundant CyP40 functions in cytoskeletal remodeling of the parasite during stationary growth phase, which is likely the basis for the aberrant morphology and the motility defect observed in *cyp40-/-* parasites.

Leishmania cyp40-/- mutants fail to establish intracellular infection.

The development of highly infectious metacyclic parasites can be mimicked by exposing promastigotes to various forms of stress, including nutritional starvation and acidification at stationary phase (da Silva and Sacks, 1987; Bate and Tetley, 1993; Zakai *et al*., 1998; Serafim *et al*., 2012). The stationary phase-specific defects of *cyp40-/-* promastigotes primed us to investigate their capacity to infect host cells. Bone marrow-derived macrophages obtained from C57BL/6 mice were incubated for 2 hours with WT, *cyp40-/-*, and add-back stationary phase promastigotes at a multiplicity of infection of 10 parasites per host cell, free parasites were removed by washing, and intracellular parasite burden was determined by nuclear staining and fluorescence microscopy at 2, 24, and 48 hours post infection. The *cyp40-/-* cells were phagocytosed at levels comparable to the controls with 80% of macrophages hosting a mean of

2.5 parasites per infected host cell (Fig. 6A). While WT and add-back parasites persisted over the 48 hours post infection period and showed intracellular proliferation as documented by the increase in number of parasites per infected macrophage (Fig. 6A, lower panel), the level of *cyp40-/-* infection was reduced by over 90% during the first 24 hours and parasites were completely eliminated by 48 hours post infection (Fig. 6A). We next tested if intracellular elimination of *cyp40-/-* parasites is caused by a susceptibility to elevated temperature or acidic pH encountered inside the host cell, or results from a defect in amastigote differentiation. CyP40 null mutant promastigotes grown at 37°C did not show any significant difference to WT and add-back parasites (Fig. S7A), and axenic amastigotes developed and proliferated normally in response to both temperature and pH shift as judged by cell counting (Fig. 6B) and assessment of expression of the axenic amastigote marker protein A2 (Fig. 6C). Thus, LdCyP40 carries essential functions for successful host cell infection independent of parasite resistance to acidic pH, elevated temperature, or amastigote development.

Functional assessment of CyP40 phosphorylation.

The failure of *cyp40-/-* parasites to establish intracellular infection provided an interesting read out to test for the function of CyP40 phosphorylation in parasite infectivity using complementation analysis. We investigated the CyP40 amino acid residues that were phosphorylated by using LC-ESI-MS/MS analysis. Axenic amastigote protein extracts from transgenic *L. donovani* over-expressing Strep::CyP40 were collected and Strep::CyP40 was enriched by affinity chromatography using streptactin agarose liquid chromatography (Fig. S5). After SDS-PAGE and Coomassie Brillant Blue staining, the band corresponding to Strep::CyP40 was extracted and subjected to phosphopeptide analysis by LC-ESI-MS/MS. MS analysis revealed that residue serine 274 (S274) of CyP40 was the only detected phosphorylation site of CyP40 in axenic amastigotes (Fig. 7A and Fig. S8). The multiple

sequence alignment of trypanosomatid CyP40 described in Fig. 1 localizes S274 to the center of the TPR motif 2 and shows that it is unique among trypanosomatids (Fig. 7B). An independent study also pointed out that S274 is phosphorylated in *L. mexicana* (Dr. Martin Wiese, University of Strathclyde, Glasgow, unpublished data). These data suggest that phosphorylation at S274 of CyP40 is *Leishmania*-specific and may have critical roles in parasite survival.

To study the relationship between CyP40 phosphorylation and parasite infectivity, an add-back line was generated expressing a serine 274 to alanine (S274A) phosphorylation site mutant version of CyP40 (Fig. 7C, left panel, and Fig. S6), which was subsequently tested for *in vitro* infectivity. We next assessed the accumulation of this mutant in the parasite phospho-protein fraction to test if elimination of S274 is sufficient to abrogate phospho-specific affinity purification of CyP40. Total protein extracts and phospho-protein enriched extracts from WT treated or not with lambda phosphatase, or add-back parasites expressing CyP40-S274A were analyzed by western blotting using anti-CyP40 antibody and anti-α-tubulin antibody for normalization of the signals. As expected, robust amounts of CyP40 were detected in the wild-type phospho-protein extracts, and this signal was strongly reduced by phosphatase treatment prior to enrichment representing background levels of CyP40 enrichment likely due to non-specific binding to the affinity matrix (Fig. 7C, right panel). The same level of background signal was obtained with CyP40-S274A confirming that this residue represents the only phosphorylation site in CyP40.

Bone marrow-derived macrophages were then infected with *cyp40-/-* promastigotes complemented with CyP40-S274A. The controls, WT, *cyp40-/-* and add-back promastigotes behaved in a similar fashion as described previously (Fig. 7D). The higher counts of infected macrophage obtained with WT parasites compared to add-back control may be due to batch-to-batch variation of parasites. The *cyp40-/-/+S274A* add-back promastigotes entered

296 macrophages and established infection at similar efficiency. The parasite number decreased in
297 the first 24 hours post infection but parasites started to multiply after 48 hours (Fig. 7D, left
298 panel). The intracellular proliferation of CyP40-WT and CyP40-S274A add-back did not show
299 any significant difference, as indicated by the number of parasites per 100 macrophages at 48
300 hours post infection (Fig. 7D, right panel). These data indicate that phosphorylation of CyP40
301 is either not important for the function of CyP40 in *Leishmania* intracellular survival, or can be
302 compensated by other co-chaperones.
303
304

Discussion

The conserved co-chaperone CyP40 participates in the formation of highly dynamic heat shock protein complexes across various eukaryotes (Pratt *et al.*, 2004; Ratajczak *et al*., 2003; Riggs *et al*., 2004; Pearl and Prodromou, 2006), and has been linked to many tissue- and organism-specific functions, including steroid receptor signaling in mammalian cells and yeast (Ratajczak *et al.*, 2009), or microRNA activity and assembly of RNA-induced silencing complexes (RISCs) in plants (Smith *et al.*, 2009; Ilki *et al*., 2012). No information is available on how this co-chaperone affects viability and infectivity of trypanosomatid pathogens, including *Leishmania*, even though parasite differentiation is triggered by environmental stress signals (Zilberstein and Shapira, 1994), has been previously linked to the formation of heat shock complexes (Morales *et al*., 2010), and is regulated by HSP90 activity (Wiesgigl and Clos, 2001). Here by utilizing a targeted null mutant approach we reveal non-redundant and essential CyP40 functions in *Leishmania* stage-specific morphogenesis, motility, and the development of infectious-stage parasites.

The superfamily of immunophilin proteins is divided into cyclophilins (CyPs) and FK-binding proteins (FKBPs) based on their interaction with the immunosuppressive drugs CsA and FK506, respectively (McCaffrey *et al*., 1993; Ho *et al*., 1996). All immunophilins share a highly conserved peptidyl-prolyl isomerase (PPIase) domain implicated in proper folding of nascent proteins (Galat, 2003). Three members of this protein family have attracted considerable interest due to their interaction with HSP90 and their implication in heat shock complex formation, CyP40, FKBP51 and FKBP52. Despite considerable differences in their sequence and structure, these proteins are functionally related though their PPIase enzymatic activity and the presence of a conserved C-terminal TPR domain that confers interaction with HSP90. By dynamically competing for HSP90 binding, both CyP40 and FKBP52 co-chaperones have been shown to establish distinct steroid hormone receptor complexes in

mammals and yeast (Pratt and Toft, 1997; Ratajczak et al., 2003; Riggs et al., 2004). The absence of steroid hormone receptor signaling in *Leishmania* and related trypanosomatids raises the question on the parasite-specific functions of CyP40.

We recently obtained first insight into the biological roles and functional diversity of *L. donovani* CyPs and FKBPs using a pharmacological approach. Treatment of *L. donovani* promastigotes and axenic amastigotes with CsA and FK506 revealed important, redundant functions of CyPs and FKBPs in promastigote proliferation and morphogenesis, but unique function of *Leishmania* CyPs in parasite thermotolerance (Yau *et al*., 2010). The direct enrichment of CyP40 from *L. donovani* extracts using immobilized CsA, the presence of a conserved TPR domain in this protein, and its stage-specific phosphorylation in axenic amastigotes (Morales *et al*., 2008; Morales *et al*., 2010) suggested important stress functions of CyP40 in *Leishmania* differentiation and thermotolerance that may be regulated at post-translational levels.

However, the CyP40 loss of function analysis performed in this study shed a substantially different light on the protein's unique functions. In contrast to CsA treated promastigotes that underwent non-synchronous cell cycle arrest at logarithmic growth phase and showed morphological changes reminiscent of axenic amastigotes, i.e. retraction of the flagellum and oval cell body (Yau *et al*., 2010), *cyp40-/-* promastigotes did not show any overt defects in cell growth or cell shape at this culture stage. Moreover, absence of CyP40 expression did neither alter the IC50 to CsA nor did it affect the phenotypic response to this inhibitor (Fig S7 and data not shown) suggesting that CyP40 is not a major target of CsA at this culture stage. Finally, *cyp40-/-* parasites did not show any overt defects in resistance to various forms of stress, including nutritional starvation, acidic pH and elevated temperatures (Fig. 6D and S7), while CsA-treated parasites underwent cell death at 37°C (Yau *et al*., 2010). Thus, in contrast to other TPR domain containing chaperones in *Leishmania*, such as STI1 (Morales *et*

355 *al*., 2010; Hombach *et al*., 2013) or SGT (Ommen *et al*., 2010), which are both essential for
356 *Leishmania* promastigote viability, CyP40 carries non-essential functions at this stage, which
357 may be redundant to other PPIases of the CyP or FKBP protein families and thus compensated
358 in the null mutant.

359 Various aspects of the *cyp40-/-* null mutant phenotype pointed at essential and non-
360 redundant CyP40 functions that were not observed during CsA treatment and thus are likely
361 independent of the CyP40 PPIase activity targeted by this inhibitor (Yau *et al*., 2010). First,
362 lack of CyP40 expression caused important morphological and structural alterations of
363 stationary phase parasites, which adopted a rounded rather then characteristic needle-shaped
364 morphology. These defects were linked to a loosening of the sub-pellicular tubulin network that
365 determines parasite morphology and provides the rigidity necessary for efficient motility
366 (Seebeck *et al*., 1990). These results point to unique CyP40 functions in regulating *Leishmania*
367 cytoskeletal dynamics. Microtubule elongation and shortening are highly dynamic events that
368 are regulated by stabilizing or destabilizing interactions (Walczak, 2000). Recently, a role of
369 the CyP40 related immunophilin FKPB52 in regulating microtubule depolymerization through
370 direct interaction with tubulin via its TPR domain has been described in rat brain (Chambraud
371 *et* al., 2007). Given the capacity of CyP40 and FKBP52 to compete for molecular partners
372 (Ratajczak *et al.*, 2003), it is possible that CyP40 interacts with microtubules and promotes
373 tubulin polymerization to counteract FKBP52-mediated depolymerization. Alternatively, the
374 requirement of CyP40 for *Leishmania* morphological integrity at stationary growth phase may
375 be indirect and caused by misfolding of client proteins that require CyP40 co-chaperone
376 function. In yeast, TPR-domain containing co-chaperones make distinct and extensive contacts
377 with HSP90 that lead to a differential modulation of HSP90 chaperone function (Ratajcak *et* al.,
378 2009). For example, displacement of STI1 from HSP90 by the yeast CyP40 homolog CPR6
379 restores ATPase activity (Pearl and Prodromou, 2006). Based on our previous observation that

380 *L. donovani* STI1 acts as a scaffolding protein to assemble highly dynamic heat shock
381 complexes (Morales *et al.,* 2010), it is possible that lack of CyP40 alters the formation and
382 activity of foldosome complexes causing the observed phenotypic consequences of CyP40
383 deletion.

384 Second, *cyp40-/-* parasites showed an important, stage-specific defect in directional
385 motility despite integrity of the 9+2 structure of the axoneme. The presence of trypanosomatid
386 CyP40 in the flagellar proteome (Oberholzer *et al*., 2011) indicates that LdCyP40 may directly
387 interact with motor components for proper folding. This possibility is supported by various
388 studies of related FKBPs showing (i) direct interaction between the FKBP52 PPIase domain
389 and the motor protein dynein via dynamitin (Silverstein *et al*., 1999; Galigniana *et al*., 2001;
390 Galigniana *et al.,* 2004), (ii) an essential role of FKBP52 for sperm tail development and
391 movement (Hong *et al*., 2007), and (iii) a requirement of FKBP12 in *Trypanosoma brucei*
392 motility (Brasseur *et* al., 2013).

393 Finally, the most striking loss-of-function phenotype of *cyp40-/-* parasites is represented
394 by the abrogation of intracellular parasite survival. While we cannot rule out that loss of
395 intracellular survival reflects a developmental defect caused by the morphological and
396 cytoskeletal alterations observed at stationary phase culture, our observations that null mutant
397 parasites are normal in viability and metacyclic marker expression, and convert normally into
398 axenic amastigotes may point to different possible scenarios. Intracellular killing of *cyp40-/-*
399 mutants may be associated with the requirement of LdCyP40 co-chaperone activity for proper
400 folding of parasite survival factors, which may confer parasite resistance to macrophage
401 cytolytic activities. Alternatively, the identification of LdCyP40 in the parasite secretome
402 (Silverman *et* al., 2008) opens the possibility that this co-chaperone may directly interact with
403 host phagolysosomal or cytoplasmic proteins to subvert host cytolytic activities and favor
404 intracellular parasite survival, a scenario reminiscent to secreted *T. cruzi* CyP19, which

405 inactivates the anti-microbial peptide trialysin of the reduviid insect vector by direct binding
406 (Kulkarni *et al.*, 2013). A third possibility is the involvement of CyP40 in the sorting of
407 exosome payload proteins, similar to the role played by the chaperone HSP100 (Silverman *et*
408 *al.*, 2010). This idea would be supported by the very similar phenotypes of CyP40 (this paper)
409 and HSP100 null mutants (Krobitsch and Clos, 1999).

410 In previous phosphoproteomics investigations we identified LdCyP40 as a major
411 amastigote-specific phosphoprotein and revealed a coordinated increase in phosphorylation of
412 all major parasite chaperones and HSPs during axenic amastigote differentiation, which
413 occurred largely at parasite-specific sites (Morales *et al*., 2008; Morales *et al*., 2010; Hem *et al*.,
414 2010). These results are compatible with the hypothesis that *Leishmania* stress protein function
415 is regulated at post-translational levels through phosphorylation by stress-activated protein
416 kinases, a possibility that is supported by the genetic validation of two phosphorylation sites in
417 *L. donovani* STI1 that are essential for parasite viability (Morales *et al*., 2010). The failure of
418 *cyp40-/-* parasites to establish intracellular infection provided a powerful read out to further test
419 this hypothesis and to assess the physiological role of CyP40 phosphorylation by site-directed
420 mutagenesis of the single CyP40 phosphorylation site. Surprisingly, although CyP40
421 phosphorylation at S274 was highly stage-specific and observed exclusively in axenic and *bona*
422 *fide* splenic amastigotes, expression of an LdCyP40 S274A mutant fully restored intracellular
423 survival of *cyp40-/-* parasites thus ruling out an essential role of this modification in
424 intracellular infection *in vitro*. The biological function of this highly conserved phosphorylation
425 site eludes us. Phosphorylation of FKBP52 disrupts the binding activity of this chaperone to
426 HSP90 and thus is required for the dynamic turnover of heat shock complexes (Miyata *et al*.,
427 1997). The S274 CyP40 phosphorylation site maps to the TPR2 sub-domain and thus may play
428 a similar role in regulating the dynamics of protein-protein interactions, but may not cause a

429 discernible phenotype due to the expression of other, functionally redundant TPR-domain
430 proteins in *Leishmania.*

431 In conclusion, null mutant analysis of LdCyP40 revealed important non-redundant
432 functions of this co-chaperone in parasite morphogenesis, cytoskeletal remodeling during
433 stationary growth phase, motility, and infectivity. How LdCyP40 carries out its parasite-
434 specific functions, and whether they depend on CyP40 isomerase and/or (co-)chaperone
435 activities remains to be elucidated. In other organisms, CyP40 exerts its function mainly
436 through binding to HSP90 (Li *et al.*, 2011). There are several lines of evidence that CyP40
437 functions in *Leishmania* may not follow this established model as isolation of HSP90
438 complexes by anti-STI1 immuno-precipitation from *L. donovani* promastigotes and axenic
439 amastigotes did not reveal LdCyP40 (Morales *et al.*, 2010), although both co-chaperones can
440 bind HSP90 simultaneously in other organisms (Li *et al.*, 2011). In addition, while the
441 LdCyP40 PPIase domain is highly conserved, the TPR domain underwent substantial
442 evolutionary modification (Yau *et al.*, 2010), which may impact on LdCyP40-HSP interactions.
443 Future studies applying structure/function analyses to assess LdCyP40 isomerase and
444 chaperone activities, combined with pull down assays and native electrophoresis, will elucidate
445 the roles of the LdCyP40 PPIase and TPR domains in *L. donovani* differentiation, virulence and
446 stress protein interaction.
447
448

Experimental procedures

Ethics statement. All animals were handled according to institutional guidelines of the Central Animal Facility of the Institut Pasteur (Paris, France) and experiments were performed in accordance with protocols approved by the animal Experimentation Ethics Committee of the Institut Pasteur (permit #03–49) and the veterinary service of the French Ministry of Agriculture (number B-75-1159, 30 May 2011). The animals were housed and handled in accordance with good animal practice as defined by FELASA (www.felasa.eu/guidelines.php).

Mice, macrophages and parasites. Wild-type C57BL/6 mice were purchased from Charles River, and were kept and treated according to the institutional guidelines for animal experiments. Bone marrow-derived macrophages (BMMs) were prepared from the femurs of 6 – 8 weeks old female mice as described (Forestier *et al.*, 2011). *Leishmania donovani* strain 1SR (MHOM/SD/62/1SR) was maintained at 25°C, pH 7.4 in supplemented M199 medium (Kapler *et al.*, 1990; Hubel *et al.*, 1997). Axenic differentiation of promastigotes was performed as described (Goyard *et al.*, 2003; Morales *et al.*, 2008).

Multiple sequences analysis. The putative cyclophilin 40 protein sequences of human, mouse, bovine, yeast and several trypanosomatids, including *L. major*, *L. infantum*, *L. braziliensis*, *T. brucei* and *T. cruzi*, were retrieved from the NCBI (http://www.ncbi.nlm.nih.gov/protein/) and TriTrypDB databases (http://tritrypdb.org/tritrypdb/) by Blast search with algorithum blastp using *L. major* cyclophilin 40 (LmjF35.4770) as a query. The retrieved sequences were aligned with ClustalW 2.0.12 and the aligned data were used to build a neighbour-joining tree and to cluster the CyP40s, using the built-in programs of Geneious version 4.8 (Larkin *et al*., 2007; Kearse *et al*., 2012; http://www.geneious.com). Matrix Blosum62 was applied as the scoring

rule for amino acid substitution (Henikoff and Henikoff, 1993). Sequence alignments with Expect (E) values less than 10^{-5} were considered significant.

Generation of *L. donovani cyp40-/-* mutants by gene replacement. Null mutant parasites were generated by sequential replacement of the endogenous *CYP40* alleles using two targeting constructs comprising puromycin and bleomycin resistance genes flanked by approximately 1000 bp of the 5' and 3'UTRs of the *L. infantum CYP40* gene (GeneDB accession number LinJ.35.4830) that were PCR amplified from *L. infantum* genomic DNA (strain MHOM/FR/91/LEM2259). Genomic DNA of parasites was extracted with Gentra Systems Puregene Tissue Core Kit A (Qiagen) according to the manufacturer's instruction.

For subsequent cloning of the 5'UTR, primer pairs CYP40-5'UTR-fwd (GGGGAATTCATTTAAATGAGATGCGGTAGATGTCCTG) and CYP40-5'UTR-rev (GGGGGTACCTGCGTGCGTGTAGGTCTAC) added EcoRI and SwaI sites (underlined) to the 5'-end, and a KpnI site to the 3'-end. For cloning of the 3'UTR, primer pairs CYP40-3'UTR-fwd (GGGGGATCCGTTGCGCCTGCCGGACAGAAC) and CYP40-3'UTR-rev (CCCAAGCTTATTTAAATGAGTGAGACGTGCACGCAAC) added BamHI site to the 5'-end, and HindIII and SwaI sites to the 3'-end. The amplified fragments were digested with EcoRI/KpnI and BamHI/HindIII and ligated into pUC19 vector digested with the same enzyme pairs yielding the constructs pUC-CYP40-5'UTR and pUC-CYP40-3'UTR. Next, the cloned 5'UTR fragment was liberated by EcoRI and KpnI digestion, ligated into pUC-CYP40-3'UTR digested with the same enzyme pair yielding the construct pUC-CYP40-5'3'UTR. For the construction of the final targeting constructs, the antibiotic resistance genes *PAC* and *BLE* were isolated from pUC-PAC and pUC-BLE after digestion with KpnI and BamHI and ligated into pUC-CYP40-5'3'UTR digested with the same enzymes, yielded the final constructs pUC-CYP40-5'PAC3' and pUC-CYP40-5'BLE3' used for *Leishmania CYP40* gene replacement.

For genetic complementation of the CyP40 null mutant, an "add-back" line was established using a knock-in strategy. The *CYP40* open reading frame was PCR amplified using primers CYP40-5'Kpn (GGGGGTACCATGCCGAACACATACTGC) and CYP40-3'BglII (GGGAGATCTTCACGAGAACATCTTCTTG), adding KpnI and BglII sites (underlined) to the 5'- and 3'-ends of the *LmCYP40,* respectively. The amplified fragment was digested with these enzymes, ligated into pUC-CYP40-3'UTR digested with KpnI and BamHI yielding the construct pUC-CYP40+3'UTR. The cloned CYP40+3'UTR was liberated by digestion with Acc65I and SwaI, the 5'-protruding end of the digested fragment was filled-in with Klenow fragment, and cloned into XbaI/BglII digested and blunt ended vector pIRmcs3+ (Hoyer *et al.*, 2004) yielding the final construct pIR-CYP40 used for integration into the small ribosomal subunit (SSU) locus of the *cyp40-/-* genome.

The plasmids were extracted from transformed *E. coli* DH5α, purified using CsCl continuous gradient centrifugation and linearized with SwaI. The targeting fragments were separated by agarose electrophoresis, purified and transfected into logarithmic promastigotes by electroporation as described (Spath *et al.*, 2000; Ommen *et al.*, 2009). Integration of gene replacement constructs was verified by PCR using the primer pairs: (P1, CATTTGGCGCTTTTCATGC; P2, ATTACATCAGACGTAATCTG; P3, TGGAAAGTGCTACCCTGGTACGTC; P4, GTGGGCTTGTACTCGGTC; P5, GGAACGGCACTGGTCAAC). PCR products were analyzed by agarose gel electrophoresis.

Site-directed mutagenesis. Cloned *L. major CYP40* in the construct pUC-CYP40+3'UTR was used as template for site-directed mutagenesis that is based on a modified PCR (Hombach *et al.*, 2013). The template was amplified by PCR using the following phosphorylated oligonucleotide pairs (mutation sites were underlined) to introduce the mutation: CYP40-S274A-fwd (GCAGTGGGCGGAGGCTCGCCACACGGCGTC) and CYP40-S274-rev

523 (TGGAGCTTGATGGCGCACATTG). The PCR products were ligated and used to transform
524 competent *E. coli* DH5α (Invitrogen). Plasmids were extracted and purified for DNA
525 sequencing to verify the mutation.
526
527 **Cell counting.** The cell density of parasite cultures were determined every 24 hours either
528 using a CASY cell counter (Schärfe System) or microscopically by counting 2% (w/v)
529 glutaraldeyhde fixed cells loaded into a Neubauer-improved cell counting chamber
530 (Marienfeld).
531
532 **Macrophage infection assays.** Isolation and differentiation of BMMs were performed as
533 described (Forestier *et al.*, 2011). The mature BMMs were treated with 20 mM EDTA for
534 detachment. The dislodged cells were resuspended in complete RPMI medium and plated
535 overnight in 24-well plates containing sterile 12-mm glass coverslips at a cell density of 1×10^5
536 cells/well. *L. donovani* promastigotes cultured for 6 days until stationary-phase ($8 – 10 \times$
537 10^7/ml), or axenic amastigotes from logarithmic growth phase ($1 – 5 \times 10^7$/ml) were washed
538 three times with plain RPMI medium and once with infection medium (0.7% BSA, 25 mM
539 HEPES [pH 7.4] in plain RPMI medium), incubated with BMMs at 37ºC with 5% CO_2 for 2
540 hours at a multiplicity of infection of 10 parasites per host cell. Extracellular parasites were
541 then removed by washing the coverslips extensively with PBS and transfer of the cover slip
542 into new 24-well plates containing 1 ml of fresh complete RPMI medium per well. This
543 washing procedure was repeated daily until 5 days post infection. The plates were incubated for
544 up to 5 days at 37ºC with 5% CO_2 during the experiment.
545
546 **Analysis of intracellular parasite burden.** Coverslips of quadruplicate experiments were
547 collected at 0, 24 and 48 hours post infection, washed once with PBS and then fixed with 4%

548 (w/v) paraformaldehyde for 15 min at room temperature. After three further washes with PBS
549 and one wash with ddH_2O, the coverslips were mounted with Mowiol medium containing
550 nuclear dye Hoechst 33342 (Invitrogen). At least 100 macrophages were imaged per coverslip
551 using Axioplan 2 wide field light microscope with the Apotome module (Carl Zeiss). Number
552 of parasites and macrophages was estimated counting host cell and parasite nuclei using ImageJ
553 (National Institute of Health, US) using a predefined pixel range for each cell type (400 to
554 infinity pixels, macrophages; 0 to 150 pixels, parasites; 100 to 200 pixels, CFSE labeled
555 parasites in case of mixed infection assay).
556
557 **Microscopic analyses.** *Giemsa staining analysis.* Parasites (1×10^6) were settled on poly-L-
558 lysine coated glass slides and air-dried overnight. The dried cells were fixed with methanol and
559 stained with Giemsa solution (Sigma) for 10 min. After rinsing with water and air-drying, the
560 slides were mounted with Immersol 518N (Carl Zeiss) and observed under an Axioplan 2 wide
561 field light microscope (Carl Zeiss). The acquired images were analyzed by Zeiss Axiovision
562 release 4.7 (Carl Zeiss) or Openlab v3.0 (Improvision).
563 *Scanning electron microscopy.* Parasites were washed twice in ice-cold PBS and then
564 fixed with 2% (w/v) glutaraldehyde (Sigma) in PBS with 0.1 M sodium cacodylate (pH 7.2).
565 Briefly, the fixed cells were treated with 1% (w/v) OsO_4 and dehydrated followed by critical-
566 point drying (CPD 7501, Polaron) and coated with gold powder (Ion Beam Coater 681, Gatan).
567 Samples were visualized with scanning electron microscope SEM 500 (Philips). For
568 cytoskeleton analysis, cells were treated with 1% Triton X-100 at 4ºC in PBS for 10 minutes to
569 strip the plasma membrane and visualize the cytoskeleton. The samples were then washed
570 twice in PBS, fixed in glutaraldehyde and processed for scanning electron microscopy in
571 standard conditions as described (Absalon *et al.*, 2008).

572 *Transmission electron microscopy.* Parasites were washed twice in ice-cold PBS and
573 then fixed with 2% (v/v) glutaraldehyde (Sigma) in PBS with 0.1 M sodium cacodylate (pH
574 7.2). The fixed cells were post-fixed in 1% (w/v) OsO_4 and then dehydrated with increasing
575 ethanol concentrations (70–100%) and embedded in EPON epoxy resin (Hexion Speciality
576 Chemicals). Ultrathin sections (~70 nm) were prepared using an Ultramicrotome (Ultra Cut E;
577 Reichert/Leica) and stained with uranyl acetate and lead citrate. Sections were analyzed using
578 the Tecnai Sprit TEM (FEI).
579
580 **Annexin V-FITC assay.** Parasites (2×10^7 cells) were washed and resuspended in 100 µl of
581 binding buffer containing 100 µg/ml of FITC conjugated annexin V (a gift from Dr. Aude
582 Foucher, Photeomix, Paris), 1 µg/ml of PI, 10 mM HEPES (pH 7.4), 140 mM NaCl and 5 mM
583 $CaCl_2$. The suspensions were incubated at room temperature for 10 min in the dark. The stained
584 cells were subjected to FACS analysis (λ_{ex} = 488 nm; λ_{em} = 515 nm [FITC] and 617 nm [PI])
585 with a FACSCalibur™ (BD Biosciences). 10,000 events were analyzed using FlowJo 8.7 (Tree
586 Star).
587
588 **SYBR Green-based semi-quantitative RT-PCR**. SHERP cDNA was amplified using forward
589 primer CGACAAGATCCAGGAGCTGAAGGAC and reversed primer
590 CCTTGATGCTCTCAACCGTGCTG). Beta actin cDNA was amplified as reference gene to
591 calculate relative expression levels of SHERP mRNA.
592
593 **Motility analysis.** For each condition, at least 3 movies were recorded (500 frames at 33 ms of
594 exposure for 16 s movies). Samples were observed in their respective culture media (cell
595 density of about 5×10^6 cells/ml in logarithmic phase or 107 cells/ml in stationary phase) under
596 a 10× objective of an inverted DMI4000 microscope (Leica). Cells were filmed using a

597 numeric camera Photometrics Evolve 512 (Photometrics). Movies were converted with the
598 MPEG Streamclip V1.9b3 software (Squared 5) and analyzed with the ICY software
599 (http://www.bioimageanalysis.org/). For each movie, at least 255 cells were simultaneously
600 tracked in silico. Mean speeds (in μm/s) were calculated from instant velocity data transferred
601 and compiled in Microsoft Excel. Statistical analyses were performed in the KaleidaGraph
602 V4.0 software (Synergy Software). Data were first filtered (number of spot detections > 3 and
603 mean speed < 100 μm/s) to exclude false tracks (non-*Leishmania* objects, dead cells and/or
604 attached cells). An ANOVA test was then performed with Tukey ad-hoc post-tests at 0.5 for
605 intergroup comparisons ($p < 0.0001$).
606
607 ***Leishmania* phosphoprotein enrichment.** Promastigotes, axenic amastigotes, and splenic
608 amastigotes derived from *Leishmania* infected hamsters, were centrifuged at 1000 × g at 4ºC
609 for 10 min. Pellets were washed twice with plain M199 medium, then resuspended in lysis
610 buffer (150 mM NaCl, 50 mM Tris-HCl pH 7.4, 1% Triton X-100, 1% benzonase, and protease
611 inhibitor cocktail [Roche]) and lysed at 4ºC for 30 min with vortexing every 10 min. The lysate
612 was then sonicated on ice for 5 min (10 seconds pulse with a 20 seconds pause) using Bioruptor
613 (Diagenode). Cell debris was removed by brief centrifugation. Protein concentration of lysates
614 was estimated by RC DC protein assay (Bio-rad) and adjusted to 0.1 mg protein/ml with lysis
615 buffer. Phosphoprotein was enriched using the Phosphoprotein purification kit (Qiagen)
616 according to the manufacturer's instructions. Briefly, 2.5 mg of total protein were loaded to the
617 equilibrated columns. Unbound proteins were removed by washing the column with 6 ml of
618 lysis buffer. Bound phosphorylated proteins were eluted with 2 ml elution buffer and
619 concentrated using Amicon Ultra-0.5 ml centrifugal filters with Ultracel® 10K membrane
620 (Millipore).
621

622 **Phosphopeptide identification.** Cell lysate extracted from transgenic *L. donovani* expressing
623 Strep::CyP40 (refer to supporting information) was separated by SDS-PAGE. Separated
624 Strep::CyP40 was trypsin-digested and diluted in loading buffer (80% ACN, 5% TFA). The
625 sample was then processed for LC-ESI-MS/MS analysis to identify phosphorylation sites, as
626 described (Morales *et al*., 2010). Briefly, digested protein was diluted in loading buffer (80%
627 ACN, 5% TFA) and loaded on TiO_2 microcolumns. After two washing steps in 10 µl loading
628 buffer and 60 µl buffer 2 (80% ACN, 1% TFA), phosphopeptides were eluted using 10 µl
629 NH_4OH (pH 12), dried, then resuspend in 10 ul of 0.1% formic acid before analyzing with a Q-
630 TOF mass spectrometer (Maxis; Bruker Daltonik GmbH, Bremen, Germany), interfaced with a
631 nano-HPLC U3000 system (Thermo Scientific, Waltham, USA). Samples were concentrated
632 with a pre-column (Thermo Scientific, C18 PepMap100, 300 μm × 5 mm, 5 μm, 100 A) at a
633 flow rate of 20 µL/min using 0.1% formic acid. After pre-concentration, peptides were
634 separated with a reversed-phase capillary column (Thermo Scientific, C18 PepMap100, 75 μm
635 × 250 mm, 3 μm, 100 A) at a flow rate of 0.3 µL/min using a two-step gradient (8 % to 28 %
636 acetonitrile in 40 min then 28 % to 42 % in 10 min), and eluted directly into the mass
637 spectrometer. Proteins were identified by MS/MS by information-dependent acquisition of
638 fragmentation spectra of multiple charged peptides and MS/MS raw data were analysed using
639 Data Analysis software (Bruker Daltonik GmbH, Bremen, Germany) to generate the peak lists.
640 The *L. major* database from GeneDB was searched using MASCOT software (Matrix Science,
641 London, UK) with the following parameters: trypsin cleavage, one missed cleavage sites
642 allowed, carbamidomethylation set as fixed modification, 10 ppm mass tolerance for MS, and
643 0.05 Da for MS/MS fragment ions. Phosphorylation (ST), Phosphorylation (Y) and oxidation
644 (M) were allowed as variable modifications. All phosphorylated peptides were first checked for
645 the presence of the major fragment ion $[MH\text{-}H_3PO_4]+$ = MH - 98 Da corresponding to the loss

646 of the phosphate moiety and identified positively by MASCOT. In addition, all MS/MS spectra
647 were carefully checked manually for assignment of phosphorylation sites.
648
649 **Western blot analysis.** Samples in 1× Laemmli buffer were separated by 10% SDS-PAGE and
650 then transferred to PVDF membranes. Rabbit anti-CyP40 antiserum (1:20000 dilution, Yau *et*
651 *al.*, 2010), mouse anti-A2 antibody (clone C9, 1:50 dilution, Zhang *et al*., 1996), mouse anti-
652 LPG antibody (clone CA74E, 1:20000 dilution, Tolson *et al.*, 1994), mouse anti-α-tubulin
653 antibody (clone B-5-1-2, 1:20000 dilution, Sigma), mouse anti-β-tubulin antibody (clone
654 KMX, 1:100 dilution, Absalon *et al.*, 2007), goat anti-mouse HRP conjugated antibody
655 (1:20000 dilution, Thermo Scientific) and goat anti-rabbit HRP conjugated antibody (1:20000
656 dilution, Thermo Scientific) were used to probe the membrane. SuperSignal West Pico
657 chemiluminescent substrate (Thermo Scientific) was added to the membranes and
658 chemiluminescent signals were revealed on X-ray films.
659
660 **Statistical analysis.** Numerical data were expressed as mean ± standard deviation. Mann-
661 Whitney U test was used to compare the significance between specific groups and $p < 0.05$ was
662 considered as statistically significant. All statistical analysis was performed using either Excel
663 2003 (Microsoft) or Prism 5.0 (GraphPad).
664
665 **Acknowledgments**
666 We thank Dirk Schmidt-Arras (University of Kiel), Gabi Ommen, Mareike Chrobak and
667 Christel Schmetz (Bernhard Nocht Institute, Hamburg) for discussion, Eric Prina for critical
668 reading of the manuscript, Claire Forestier and Evie Melanitou (Institut Pasteur) for advices on
669 macrophage experiment, Emanuelle Perret from the Institut Pasteur Imaging platform for
670 advice on fluorescence microscopy, and Abdelkader Namane from the Institut Pasteur

671 Proteomics platform for protein determination. This work was supported by the Institut Pasteur,
672 Réseau International des Instituts Pasteur, Centre Nationale de Recherche Scientifique, the 7th
673 Framework Programme of the European Commission through a grant to the LEISHDRUG
674 Project (223414), the Fondation de Médicale Recherche and Deutscher Akademischer
675 Austausch Dienst, and the French Government's Investissements d'Avenir program:
676 Laboratoire d'Excellence 'Integrative Biology of Emerging Infectious Diseases' (grant no.
677 ANR-10-LABX-62-IBEID).

678

679

680

681 **Figure legends**

682 **Fig 1. *L. donovani* CyP40 is a conserved chaperone and shows amastigote-specific**
683 **phosphorylation.** *(A) Amino acid sequence analysis of Leishmania CyP40.* Multiple alignment
684 of CyP40 amino acid sequences of mammal (human, mouse and bovine), trypanosomatid
685 (*Leishmania* and *Trypanosoma*) and yeast was performed using ClustalW as described in
686 experimental procedures. CLD/PPIase (cyclophilin-like domain/PPIase) and TPR domains are
687 indicated. Degree of residue conservation is represented by the colour code (green, 80-100%
688 conserved; yellow, 30-80% conserved; red, 10-30% conserved). *, key residues for cyclosporin
689 A binding and PPIase activity; ^, key residues for chaperone function; Δ, key residues for
690 HSP90 binding. Accession numbers: M.mus, NP_080628.1; H.sap, NP_005029.1; B. tau,
691 NP_776578.1; S.cer, NP_013317.1; T.cru, TcCLB.506885.400; T.bru, Tb927.9.9780; L.bra,
692 LbrM34.4730; L.mex, LmxM34.4770; L.inf, LinJ35.4830; L.maj, LmjF35.4770. *(B) Western*
693 *blot analysis.* Phosphoproteins of *in vitro* cultivated *L. donovani* promastigote (pro), axenic
694 amastigote (ama, ax), and amastigotes harvested from infected hamster spleen (sp) were
695 enriched using a Phosphoprotein purification kit (Qiagen). Total and phosphoprotein

696 extractswere analyzed by Western blotting using anti-CyP40 antiserum and anti-α-tubulin
697 antibody for normalization.
698
699 **Fig. 2. CyP40 null mutant parasites are viable in culture.** *(A) Targeted replacement and*
700 *add-back strategies.* Targeting constructs comprising bleomycin (*BLE*) and puromycin (*PAC*)
701 resistance genes flanked by the *CYP40* 5' and 3' untranslated regions (UTRs) were used for
702 deletion of the genomic *CYP40* alleles. A targeting construct containing the nourseothricin
703 resistance gene (*SAT*) and the *Leishmania major CYP40* open reading frame (ORF) flanked by
704 the *L. major* small ribosomal subunit homology regions (*LmSSU*) were used for restoring
705 CyP40 expression in the *cyp40-/-* parasites. Primers specific for amplifying *CYP40* (P1/P4), the
706 resistance genes *PAC* (P2/P4) and *BLE* (P3/P4), and the *SSU* locus (P1/P5) are indicated. *(B)*
707 *Validation of homologous recombination events by PCR analysis.* Genomic DNA of wild-type
708 (WT), heterozygous CyP40 null mutant (-/+), homozygous CyP40 null mutant (-/-) and CyP40
709 add-back (-/-/+) was subjected to diagnostic PCR analysis using the indicated primer pairs
710 (P_xP_y) to amplify the endogenous CyP40 ORF (*CYP*), the *CYP40* ORF integrated into the
711 ribosomal locus (*SSU*), and the bleomycin (*BLE*) and puromycin (*PAC*) resistance genes. *(C)*
712 *Western blot analysis.* Total protein from wild-type (WT) and CyP40 null mutant (-/-) and add-
713 back (-/-/+) were extracted and analyzed by western blotting using anti-CyP40 (CyP, upper
714 panel) and anti-α-tubulin antibodies (Tub, lower panel). The molecular weight of marker
715 proteins in kDa is indicated.
716
717 **Fig. 3. Stationary *cyp40-/-* promastigotes show altered morphology.** *(A) Morphological*
718 *analysis.* Promastigotes of wild-type (WT), *cyp40-/-* (clones 4 and 5) and the respective *cyp40-*
719 */-/+* clones from logarithmic and stationary growth phase were stained with Giemsa and
720 analyzed using a light microscope (Leica) controlled by OpenLab v3.0 (Improvision). Scale bar

721 represents 10 μm. *(B, C) Electron microscopy analysis*. Promastigotes from stationary growth
722 phase were fixed and processed for either scanning (B) or transmission EM (C) as described in
723 Materials and Methods. Scale bar represents 10 μm in the scanning EM panels and 500 nm in
724 the transmission EM panels. *(D) Cell viability determination.* Stationary promastigotes of wild-
725 type (WT) and *cyp40-/-* (-/-) from 6 days cultures were stained with propidium iodide (PI, 1
726 μg/ml) and annexin V-FITC (1 μg/ml) for 10 min, and respective fluorescence intensities were
727 analyzed by FACS. Numbers at the lower-right quadrant represent percentage of apoptotic cells
728 (PI-, Annexin V-FITC+), while numbers at the upper-right quadrant represent percentage of
729 dead cells (PI+, Annexin V-FITC+).
730
731 **Fig 4. Growth characterization of Cyp40 null mutant promastigotes.** *(A) In vitro growth*
732 *curve of cyp40-/- mutants.* Promastigotes of wild-type (WT), *cyp40-*/- (-/-) and *cyp40-*/-/+ (-/-/+)
733 were cultured at 25ºC, pH 7.4 for 120 hours. Aliquots of culture were collected every 24 hours
734 and cell density was measured with a CASY cell counter. *(B) Western blot analysis of LPG*
735 *expression.* 5×10^6 wild-type or *cyp40-/-* parasites from logarithmic (log) or stationary (stat)
736 cell culture were subjected to western blot analysis using anti-LPG antibody. *(C) RT-PCR of*
737 *SHERP expression.* Total RNA of the wild-type (black), cyp40-/- (white) and cyp40-/-/+ (gray)
738 were extracted, reverse transcribed, and amplified with SHERP specific primer. β -tubulin was
739 amplified with specific primers as reference gene. Relative expression levels of SHERP mRNA
740 was analyzed using semi-quantitative RT-PCR.
741
742 **Fig. 5. Analyses of motility and cytoskeleton of stationary phase *cyp40-/-* promastigote.** *(A,*
743 *B) Motility analysis.* Motility tracks were established for logarithmic (log) and stationary phase
744 (stat) wild-type (WT), *cyp40-/-* (-/-) and *cyp40-/-/+* (-/-/+) promastigotes. For each condition, at
745 least 3 movies were recorded for the simultaneous *in silico* tracking of at least 255 cells per

746 movie. Mean speed (in μm/s) was calculated from instant velocity data and graphically
747 represented in left panel with SD bars. *ANOVA test, $p < 0.0001$. n=735 for WT Log and 737
748 for WT Stat, n=746 for -/- Log and 747 for -/- Stat, n=741 for -/-/+ Log and 742 for -/-/+ Stat.
749 Characteristic tracks are shown in Fig. 5B. *(C) Flagellar ultrastructure of stationary WT and*
750 *cyp40-/- promastigotes*. Scale bar represents 100 nm. *(D) Cytoskeleton analysis.* Wild-type
751 (WT) and *cyp40-/-* (-/-) stationary promastigotes were treated with 1% Triton X-100 at 4°C in
752 PBS for 10 minutes to strip the plasma membrane and visualize the parasite cytoskeleton.
753 Samples were washed twice in PBS, fixed and processed for scanning electron microscopy as
754 described (Absalon *et al*., 2008). Scale bar represents 100 nm. *(E) Western blot analysis of*
755 *HSPs and tubulin expression.* Crude lysate of 5 x 10^6 parasites obtained from logarithmic (log)
756 or stationary (stat) cultures were boiled directly in Laemmli buffer and separated on NuPAGE
757 4-12% gel, and transferred to PVDF membranes. The membranes were then incubated with
758 mouse monoclonal IgG clone B-5-1-2 antibody for α-tubulin or monoclonal IgG clone KMX
759 antibody for β-tubulin, and subsequently incubated with anti-mouse IgG conjugated with HRP.
760 Signals were revealed by chemiluminescence after addition of substrate. The molecular weight
761 of marker proteins in kDa is indicated.
762
763 **Fig. 6. Intracellular survival and axenic differentiation of the *cyp40-/-* null mutants.** *(A)*
764 *Macrophage infection assay.* BMMs from C57BL/6 mice were infected with stationary phase
765 promastigotes of *L. donovani* wild-type (WT, O), *cyp40*-/- (clone 4, □, and 5, ■) or *cyp40*-/-/+
766 (Δ) for 2 hours, and parasite burden was analyzed at 0, 24 and 48 hours post-infection by
767 nuclear staining with Hoechst 33342 and fluorescence microscopy. Results are representative
768 of three triplicate experiments with standard deviation denoted by the bars is shown. *(B)* In
769 vitro *growth curve of cyp40-/- axenic amastigotes.* Promastigotes of wild-type (WT), *cyp40*-/-
770 (-/-) and *cyp40*-/-/+ (-/-/+) were induced for axenic differentiation at 37ºC, pH 5.5 for 72 hours,

771 and amastigote growth was monitored following inoculation of 2 x 10^6 axenic amastigotes into
772 fresh medium and daily determination of cell density with a CASY cell counter. *(C) A2 marker*
773 *protein expression analysis.* Extracts from wild-type (WT), *cyp40*-/- (-/-) and *cyp40*-/-/+ (-/-/+)
774 axenic amastigotes 72 hours after incubation under differentiation-inducing conditions were
775 subjected to western blot analysis using an axenic amastigote marker A2-specific monoclonal
776 antibody (upper panel). Equal loading was controlled by Coomassie staining (lower panel). The
777 molecular weight of marker proteins in kDa is indicated.
778
779 **Fig 7. Effect of phosphorylation of CyP40 on *Leishmania* intracellular survival.** *(A, B)*
780 *Phosphorylation site identification. (A)* Peptide 270LQQWSEAR277 (m/z 1098.49) was
781 identified in LC-ESI-MS/MS analysis of *L. major* Strep::CyP40 peptides after tryptic digestion
782 and TiO_2 enrichment and Ser274 was identified as a phosphorylated residue. *, fragment ions
783 arising from loss of ammonia (-17 Da); pS, phosphorylated serine. *(B) Multiple sequence*
784 *alignment of L. major CyP40 phosphoresidue.* Sequence segments encompassing CyP40
785 phosphorylation site of mouse, human, bovine, yeast, two *Trypanosoma* (*T. cruzi*, *T. brucei*),
786 four *Leishmania* species (*L. braziliensis*, *L. mexicana*, *L. infantum*, *L. major*) were analyzed
787 with ClustalW. The phospho-residue Ser274 of *L. major* CyP40 is marked by an asterisk (*).
788 *(C) Analysis of the CyP40-S274A add-back line by western blotting.* Total protein (left panel)
789 from wild-type (WT) and CyP40 null mutant (-/-) and Cyp40-WT and CyP40-S274A add-back
790 lines (-/-/+ and S274A, respectively), and enriched phosphoprotein extracts (right panel) of
791 axenic amastigotes of *L. donovani* wild-type (WT) and *cyp40-/-/+S274A* (S274A) were
792 analyzed. As background control of the phosphoprotein enrichment, 2 mg of the WT total
793 extract were first treated with 8000 units of lambda phosphatase (ΛPP) for 2 hours at 30°C. The
794 ΛPP-treated sample was then subjected to phosphoprotein enrichment. The total and
795 phosphoprotein (Phospho) extracts of the parasites were analyzed by Western blotting using

796 anti-CyP40 antiserum and anti-α-tubulin antibody. The molecular weight of marker proteins in
797 kDa is indicated. *(D) Macrophage infection assay.* BMMs from C57BL/6 mice were infected
798 for 2 hours with stationary phase promastigotes of *L. donovani* wild-type (WT, O), *cyp40-/-* (-/-
799 , □) or CyP40-WT and CyP40-S274A add-backs (respectively -/-/+, Δ and -/-/+S/A, ▼) and
800 parasite burden was at 0, 24 and 48 hours post-infection by nuclear staining with Hoechst
801 33342 and fluorescence microscopy. Result is presented as percentage infected BMMs (left
802 panel, one representative triplicate experiment with standard deviation denoted by the bars is
803 shown), and number of parasites per 100 BMMs at 48 hours post-infection (right panels, results
804 of one representative triplicate experiment with standard deviation denoted by the bars is
805 shown).
806
807
808
809 **References**

810 Absalon, S., Kohl, L., Branche, C., Blisnick, T., Toutirais, G., Rusconi, F., Cosson, J.,
811 Bonhivers, M., Robinson, D., and Bastin, P. (2007) Basal body positioning is controlled by
812 flagellum formation in *Trypanosoma brucei*. *PLoS ONE* **2:** e437.
813 Absalon, S., Blisnick, T., Bonhivers, M., Kohl, L., Cayet, N., Toutirais, G.*, et al.* (2008)
814 Flagellum elongation is required for correct structure, orientation and function of the
815 flagellar pocket in *Trypanosoma brucei*. *J Cell Sci* **121:** 3704-3716.
816 Barak, E., Amin-Spector, S., Gerliak, E., Goyard, S., Holland, N. and Zilberstein, D. (2005)
817 Differentiation of *Leishmania donovani* in host-free system: analysis of signal perception
818 and response. *Mol Biochem Parasitol* **141:** 99-108.
819 Barik, S. (2006) Immunophilins: for the love of proteins. *Cell Mol Life Sci* **63:** 2889-2900.

820 Bates, P.A., and Tetley, L. (1993) *Leishmania mexicana*: Induction of metacyclogenesis by
821 cultivation of promastigotes at acidic pH. *Exp Parasitol* **76:** 412–423.
822 Brasseur, A., Rotureau, B., Vermeersch, M., Blisnick, T., Salmon, D., Bastin, P., Pays, E.,
823 Vanhamme, L., and Pérez-Morga, D. (2013) *Trypanosoma brucei* FKBP12 differentially
824 controls motility and cytokinesis in procyclic and bloodstream forms. *Euk Cell* **12:** 168–181.
825 Chambraud, B., Belabes, H., Fontaine-Lenoir, V., Fellous, A. and Baulieu, E.E. (2007) The
826 immunophilin FKBP52 specifically binds to tubulin and prevents microtubule formation.
827 *FASEB J* **21:** 2787-2797.
828 Chappell, L.H. and Wastling, J.M. (1992) Cyclosporin A: antiparasite drug, modulator of the
829 host-parasite relationship and immunosuppressant. *Parasitology* **105 Suppl:** S25-40.
830 Cunningham, M.L., Titus, R.G., Turco, S.J. and Beverley, S.M. (2001) Regulation of
831 differentiation to the infective stage of the protozoan parasite *Leishmania major* by
832 tetrahydrobiopterin. *Science* **292:** 285-287.
833 da Silva, R. and Sacks, D.L. (1987) Metacyclogenesis is a major determinant of *Leishmania*
834 promastigote virulence and attenuation. *Infect Immun* **55:** 2802-2806.
835 Drummelsmith, J., Brochu, V., Girard, I., Messier, N. and Ouellette, M. (2003) Proteome
836 mapping of the protozoan parasite *Leishmania* and application to the study of drug targets
837 and resistance mechanisms. *Mol Cell Proteomics* **2:** 146-155.
838 Duina, A.A., Marsh, J.A. and Gaber, R.F. (1996) Identification of two CyP-40-like cyclophilins
839 in *Saccharomyces cerevisiae*, one of which is required for normal growth. *Yeast* **12:** 943-952.
840 Forestier, C.L., Machu, C., Loussert, C., Pescher, P. and Spath, G.F. (2011) Imaging host cell-
841 *Leishmania* interaction dynamics implicates parasite motility, lysosome recruitment, and
842 host cell wounding in the infection process. *Cell Host Microbe* **9:** 319-330.
843 Galat, A. (2003) Peptidylprolyl cis/trans isomerases (immunophilins): biological diversity--
844 targets--functions. *Curr Top Med Chem* **3:** 1315–1347.

845 Galigniana, M.D., Radanyi, C., Renoir, J.M., Housley, P.R., and Pratt, W.B. (2001) Evidence
846 that the peptidylprolyl isomerase domain of the hsp90-binding immunophilin FKBP52 is
847 involved in both dynein interaction and glucocorticoid receptor movement to the nucleus. *J*
848 *Biol Chem* **276:** 14884–14889.
849 Galigniana, M.D., Morishima, Y., Gallay, P.A., and Pratt, W.B. (2004) Cyclophilin-A is bound
850 through its peptidylprolyl isomerase domain to the cytoplasmic dynein motor protein
851 complex. *J Biol Chem* **279:** 55754–55759.
852 Gannavaram, S., and Debrabant, A. (2012) Programmed cell death in *Leishmania*: biochemical
853 evidence and role in parasite infectivity. *Front Cell Infect Microbiol* **2:** 95.
854 Goyard, S., Segawa, H., Gordon, J., Showalter, M., Duncan, R., Turco, S.J. and Beverley, S.M.
855 (2003) An *in vitro* system for developmental and genetic studies of *Leishmania donovani*
856 phosphoglycans. *Mol Biochem Parasitol* **130:** 31-42.
857 Hem, S., Gherardini, P.F., Osorio y Fortea, J., Hourdel, V., Morales, M.A., Watanabe, R.*, et al.*
858 (2010) Identification of *Leishmania*-specific protein phosphorylation sites by LC-MS/MS
859 and comparative genomics analyses. *Proteomics* **10:** 3868-3883.
860 Henikoff, S., and Henikoff, J.G. (1993) Performance evaluation of amino acid substitution
861 matrices. *Proteins* **17:** 49–61.
862 Ho, S., Clipstone, N., Timmermann, L., Northrop, J., Graef, I., Fiorentino, D., Nourse, J., and
863 Crabtree, G.R. (1996) The mechanism of action of cyclosporin A and FK506. *Clin Immunol*
864 *Immunopathol* **80:** S40–S45.
865 Hoffmann, K. and Handschumacher, R.E. (1995) Cyclophilin-40: evidence for a dimeric
866 complex with hsp90. *Biochem J* **307:** 5-8.
867 Hombach, A., Ommen, G., Chrobak, M., and Clos, J. (2012) The Hsp90-Sti1 Interaction is
868 Critical for Leishmania donovani Proliferation in Both Life Cycle Stages. *Cell Microbiol*
869 (Epub ahead of print)

870 Hong, J., Kim, S.T., Tranguch, S., Smith, D.F., and Dey, S.K. (2007) Deficiency of co-
871 chaperone immunophilin FKBP52 compromises sperm fertilizing capacity. *Reproduction*
872 **133:** 395–403.
873 Hoyer, C., Zander, D., Fleischer, S., Schilhabel, M., Kroener, M., Platzer, M. and Clos, J. (2004)
874 A *Leishmania donovani* gene that confers accelerated recovery from stationary phase growth
875 arrest. *Int J Parasitol* **34:** 803-811.
876 Hubel, A., Krobitsch, S., Horauf, A. and Clos, J. (1997) *Leishmania major* Hsp100 is required
877 chiefly in the mammalian stage of the parasite. *Mol Cell Biol* **17:** 5987 - 5995.
878 IIki, T., Yoshikawa, M., Meshi, T., and Ishikawa, M. (2012) Cyclophilin 40 facilitates HSP90-
879 mediated RISC assembly in plants. *EMBO J* **31:** 267–278.
880 Kapler, G.M., Coburn, C.M. and Beverley, S.M. (1990) Stable transfection of the human
881 parasite *Leishmania major* delineates a 30-kilobase region sufficient for extrachromosomal
882 replication and expression. *Mol Cell Biol* **10:** 1084-1094.
883 Kearse, M., Moir, R., Wilson, A., Stones-Havas, S., Cheung, M., Sturrock, S., Buxton, S.,
884 Cooper, A., Markowitz, S., Duran, C., et al. (2012) Geneious Basic: an integrated and
885 extendable desktop software platform for the organization and analysis of sequence data.
886 *Bioinformatics* **28:** 1647–1649.
887 Krobitsch, S., and Clos, J. (1999) A novel role for 100 kD heat shock proteins in the parasite
888 *Leishmania donovani*. *Cell Stress Chaperones* **4:** 191–198.
889 Kulkarni, M.M., Karafova, A., Kamysz, W., Schenkman, S., Pelle, R., and McGwire, B.S.
890 (2013) Secreted trypanosome cyclophilin inactivates lytic insect defense peptides and
891 induces parasite calcineurin activation and infectivity. *J Biol Chem* **288:** 8772–8784.
892 Larkin, M.A., Blackshields, G., Brown, N.P., Chenna, R., McGettigan, P.A., McWilliam, H.,
893 Valentin, F., Wallace, I.M., Wilm, A., Lopez, R., et al. (2007) Clustal W and Clustal X
894 version 2.0. *Bioinformatics* **23:** 2947–2948.

895 Laubach, V.E., Shesely, E.G., Smithies, O. and Sherman, P.A. (1995) Mice lacking inducible
896 nitric oxide synthase are not resistant to lipopolysaccharide-induced death. *Proc Natl Acad*
897 *Sci U S A* **92:** 10688-10692.
898 Lee, N., Bertholet, S., Debrabant, A., Muller, J., Duncan, R., and Nakhasi, H.L. (2002)
899 Programmed cell death in the unicellular protozoan parasite *Leishmania*. *Cell Death Differ*
900 **9:** 53–64.
901 Li, J., Richter, K. and Buchner, J. (2011) Mixed Hsp90-cochaperone complexes are important
902 for the progression of the reaction cycle. *Nat Struct Mol Biol* **18:** 61-66.
903 Mark, P.J., Ward, B.K., Kumar, P., Lahooti, H., Minchin, R.F. and Ratajczak, T. (2001) Human
904 cyclophilin 40 is a heat shock protein that exhibits altered intracellular localization
905 following heat shock. *Cell Stress Chaperones* **6:** 59-70.
906 McCaffrey, P.G., Perrino, B.A., Soderling, T.R., and Rao, A. (1993) NF-ATp, a T lymphocyte
907 DNA-binding protein that is a target for calcineurin and immunosuppressive drugs. *J Biol*
908 *Chem* **268:** 3747–3752.
909 Miyata, Y., Chambraud, B., Radanyi, C., Leclerc, J., Lebeau, M.C., Renoir, J.M., Shirai, R.,
910 Catelli, M.G., Yahara, I., and Baulieu, E.E. (1997) Phosphorylation of the
911 immunosuppressant FK506-binding protein FKBP52 by casein kinase II: regulation of
912 HSP90-binding activity of FKBP52. *Proc Natl Acad Sci U S A* **94:** 14500–14505.
913 Mojtahedi, Z., Clos, J. and Kamali-Sarvestani, E. (2008) *Leishmania major*: Identification of
914 developmentally regulated proteins in procyclic and metacyclic promastigotes. *Exp*
915 *Parasitol* **119:** 422-429.
916 Mok, D., Allan, R.K., Carrello, A., Wangoo, K., Walkinshaw, M.D., and Ratajczak, T. (2006)
917 The chaperone function of cyclophilin 40 maps to a cleft between the prolyl isomerase and
918 tetratricopeptide repeat domains. *FEBS Lett* **580:** 2761–2768.

919 Morales, M.A., Renaud, O., Faigle, W., Shorte, S.L. and Spath, G.F. (2007) Over-expression of
920 *Leishmania major* MAP kinases reveals stage-specific induction of phosphotransferase
921 activity. *Int J Parasitol* **37:** 1187-1199.
922 Morales, M.A., Watanabe, R., Laurent, C., Lenormand, P., Rousselle, J.C., Namane, A. and
923 Spath, G.F. (2008) Phosphoproteomic analysis of *Leishmania donovani* pro- and amastigote
924 stages. *Proteomics* **8:** 350-363.
925 Morales, M.A., Watanabe, R., Dacher, M., Chafey, P., Osorio y Fortea, J., Scott, D.A.*, et al.*
926 (2010) Phosphoproteome dynamics reveal heat-shock protein complexes specific to the
927 *Leishmania donovani* infectious stage. *Proc Natl Acad Sci U S A* **107:** 8381-8386.
928 Oberholzer, M., Langousis, G., Nguyen, H.T., Saada, E.A., Shimogawa, M.M., Jonsson, Z.O.,
929 Nguyen, S.M., Wohlschlegel, J.A., and Hill, K.L. (2011) Independent analysis of the
930 flagellum surface and matrix proteomes provides insight into flagellum signaling in
931 mammalian-infectious *Trypanosoma brucei*. *Mol Cell Proteomics* **10:** M111.010538.
932 Ommen, G., Lorenz, S. and Clos, J. (2009) One-step generation of double-allele gene
933 replacement mutants in *Leishmania donovani*. *Int J Parasitol* **39:** 541-546.
934 Parodi-Talice, A., Monteiro-Goes, V., Arrambide, N., Avila, A.R., Duran, R., Correa, A.*, et al.*
935 (2007) Proteomic analysis of metacyclic trypomastigotes undergoing *Trypanosoma cruzi*
936 metacyclogenesis. *J Mass Spectrom* **42:** 1422-1432.
937 Pearl, L.H., and Prodromou, C. (2000) Structure and *in vivo* function of Hsp90. *Curr Opin*
938 *Struct Biol* **10:** 46–51.
939 Pearl, L.H., and Prodromou, C. (2006) Structure and mechanism of the Hsp90 molecular
940 chaperone machinery. *Annu Rev Biochem* **75:** 271–294.
941 Pollock, J.D., Williams, D.A., Gifford, M.A., Li, L.L., Du, X., Fisherman, J.*, et al.* (1995)
942 Mouse model of X-linked chronic granulomatous disease, an inherited defect in phagocyte
943 superoxide production. *Nat Genet* **9:** 202-209.

944 Pratt, W.B., and Toft, D.O. (1997) Steroid receptor interactions with heat shock protein and
945 immunophilin chaperones. *Endocr Rev* **18:** 306–360.
946 Pratt, W.B., and Dittmar, K.D. (1998) Studies with purified chaperones advance the
947 understanding of the mechanism of glucocorticoid receptor-hsp90 heterocomplex assembly.
948 *Trends Endocrinol Metab* **9:** 244–252.
949 Pratt, W.B., Galigniana, M.D., Harrell, J.M. and DeFranco, D.B. (2004) Role of hsp90 and the
950 hsp90-binding immunophilins in signalling protein movement. *Cell Signal* **16:** 857-872.
951 Ratajczak, T., Ward, B.K., and Minchin, R.F. (2003) Immunophilin chaperones in steroid
952 receptor signalling. *Curr Top Med Chem* **3:** 1348–1357.
953 Ratajczak, T., Ward, B.K., Cluning, C. and Allan, R.K. (2009) Cyclophilin 40: An Hsp90-
954 cochaperone associated with apo-steroid receptors. *Int J Biochem Cell Biol* **41:** 1652-1655.
955 Riggs, D.L., Cox, M.B., Cheung-Flynn, J., Prapapanich, V., Carrigan, P.E., and Smith, D.F.
956 (2004) Functional specificity of co-chaperone interactions with Hsp90 client proteins. *Crit*
957 *Rev Biochem Mol Biol* **39:** 279–295.
958 Rosenzweig, D., Smith, D., Opperdoes, F., Stern, S., Olafson, R.W. and Zilberstein, D. (2008)
959 Retooling *Leishmania* metabolism: from sand fly gut to human macrophage. *FASEB J* **22:**
960 590-602.
961 Sacks, D.L. and Perkins, P.V. (1984) Identification of an infective stage of *Leishmania*
962 promastigotes. *Science* **223:** 1417-1419.
963 Seeback, T., Hemphill, A., and Lawson, D. (1990) The cytoskeleton of trypanosomes.
964 *Parasitol Today* **6:** 49–52.
965 Serafim, T.D., Figueiredo, A.B., Costa, P.A.C., Marques-da-Silva, E.A., Gonçalves, R., de
966 Moura, S.A.L., Gontijo, N.F., da Silva, S.M. et al. (2012) *Leishmania* metacyclogenesis is
967 promoted in the absence of purines. *PLoS Negl Trop Dis* **6:** e1833.

968 Silverman, J.M., Chan, S.K., Robinson, D.P., Dwyer, D.M., Nandan, D., Foster, L.J., and
969 Reiner, N.E. (2008) Proteomic analysis of the secretome of *Leishmania donovani*. *Genome*
970 *Biol* **9:** R35.
971 Silverman, J.M., Clos, J., Horakova, E., Wang, A.Y., Wiesgigl, M., Kelly, I., Lynn, M.A.,
972 McMaster, W.R., Foster, L.J., Levings, M.K., et al. (2010) *Leishmania* exosomes modulate
973 innate and adaptive immune responses through effects on monocytes and dendritic cells. *J*
974 *Immunol* **185:** 5011–5022.
975 Silverstein, A.M., Galigniana, M.D., Kanelakis, K.C., Radanyi, C., Renoir, J.M., and Pratt,
976 W.B. (1999) Different regions of the immunophilin FKBP52 determine its association with
977 the glucocorticoid receptor, hsp90, and cytoplasmic dynein. *J Biol Chem* **274:** 36980–36986.
978 Smith, M.R., Willmann, M.R., Wu, G., Berardini, T.Z., Möller, B., Weijers, D. and Poethig,
979 R.S. (2009) Cyclophilin 40 is required for microRNA activity in Arabidopsis. *Proc Natl*
980 *Acad Sci U S A* **106:** 5424-5429.
981 Spath, G.F., Epstein, L., Leader, B., Singer, S.M., Avila, H.A., Turco, S.J. and Beverley, S.M.
982 (2000) Lipophosphoglycan is a virulence factor distinct from related glycoconjugates in the
983 protozoan parasite *Leishmania major*. *Proc Natl Acad Sci U S A* **97:** 9258-9263.
984 Tolson, D.L., Schnur, L.F., Jardim, A. and Pearson, T.W. (1994) Distribution of
985 lipophosphoglycan-associated epitopes in different *Leishmania* species and in African
986 trypanosomes. *Parasitol Res* **8:** 537-542.
987 Uezato, H., Kato, H., Kayo, S., Hagiwara, K., Bhutto, A., Katakura, K., Nonaka, S., and
988 Hashiguchi, Y. (2005) The attachment and entry of *Leishmania* (*Leishmania*) *major* into
989 macrophages: observation by scanning electron microscope. *J Dermatol* **32:** 534–540.
990 Walczak, C.E. (2000) Microtubule dynamics and tubulin interacting proteins. *Curr Opin Cell*
991 *Biol* **12:** 52–56.

992 Walters, L.L., Modi, G.B., Chaplin, G.L., and Tesh, R.B. (1989) Ultrastructural development of
993 *Leishmania chagasi* in its vector, *Lutzomyia longipalpis* (Diptera: Psychodidae). *Am J Trop*
994 *Med Hyg* **41:** 295–317.
995 Walters, L.L., Irons, K.P., Chaplin, G., and Tesh, R.B. (1993) Life cycle of *Leishmania major*
996 (Kinetoplastida: Trypanosomatidae) in the neotropical sand fly *Lutzomyia longipalpis*
997 (Diptera: Psychodidae). *J Med Entomol* **30:** 699–718.
998 Ward, B.K., Allan, R.K., Mok, D., Temple, S.E., Taylor, P., Dornan, J et al. (2002) A structure-
999 based mutational analysis of cyclophilin 40 identifies key residues in the core
1000 tetratricopeptide repeat domain that mediate binding to Hsp90. *J Biol Chem* **277:** 40799–
1001 40809.
1002 Warth, R., Briand, P.A. and Picard, D. (1997) Functional analysis of the yeast 40 kDa
1003 cyclophilin Cyp40 and its role for viability and steroid receptor regulation. *Biol Chem* **378:**
1004 381-391.
1005 Weisman, R., Creanor, J. and Fantes, P. (1996) A multicopy suppressor of a cell cycle defect in
1006 *S. pombe* encodes a heat shock inducible 40 kDa cyclophilin-like protein. *EMBO J* **15:** 447-
1007 456.
1008 Wiesgigl, M. and Clos, J. (2001) Heat Shock Protein 90 Homeostasis Controls Stage
1009 Differentiation in Leishmania donovani. *Mol Biol Cell* **12:** 3307-3316.
1010 Yau, W.L., Blisnick, T., Taly, J.F., Helmer-Citterich, M., Schiene-Fischer, C., Leclercq, O.*, et*
1011 *al.* (2010) Cyclosporin A treatment of *Leishmania donovani* reveals stage-specific functions
1012 of cyclophilins in parasite proliferation and viability. *PLoS Negl Trop Dis* **4:** e729.
1013 Zakai, H.A., Chance, M.L. and Bates, P.A. (1998) *In vitro* stimulation of metacyclogenesis in
1014 *Leishmania braziliensis, L. donovani, L. major* and *L. mexicana*. *Parasitology* **116:** 305-309.

1015 Zhang, W.W., Charest, H., Ghedin, E. and Matlashewski, G. (1996) Identification and
1016 overexpression of the A2 amastigote-specific protein in *Leishmania donovani*. *Mol Biochem*
1017 *Parasitol* **78:** 79-90.
1018 Zilberstein, D. and Shapira, M. (1994) The role of pH and temperature in the development of
1019 *Leishmania* parasites. *Annu Rev Microbiol* **48:** 449-470.
1020
1021
1022
1023
1024

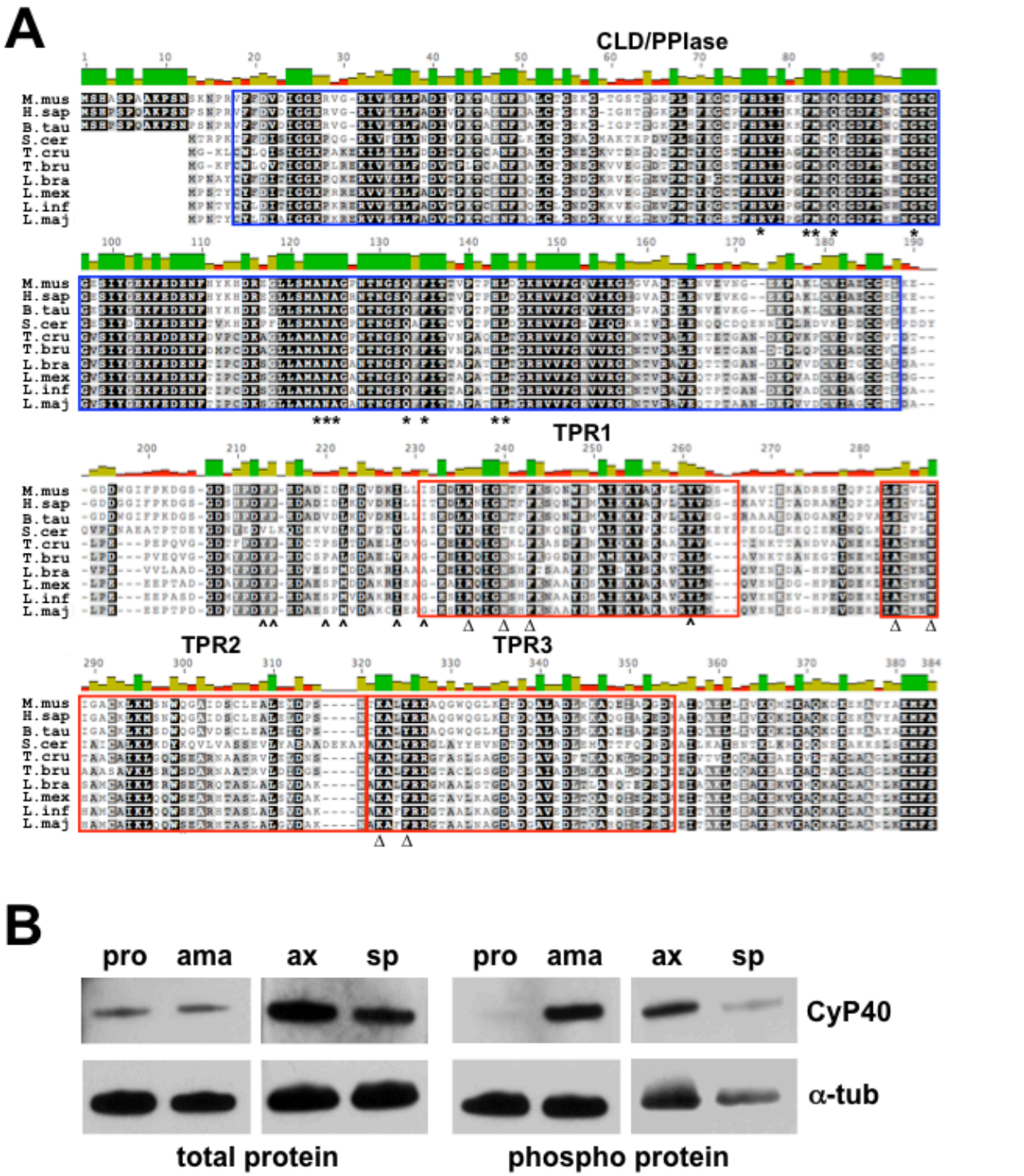
A
CLD/PPIase
TPR1
TPR2
TPR3
M.mus
H.sap
B.tau
S.cer
T.cru
T.bru
L.bra
L.mex
L.inf
L.maj
B
pro
ama
ax
sp
pro
ama
ax
sp
CyP40
α-tub
total protein
phospho protein

Figure 1

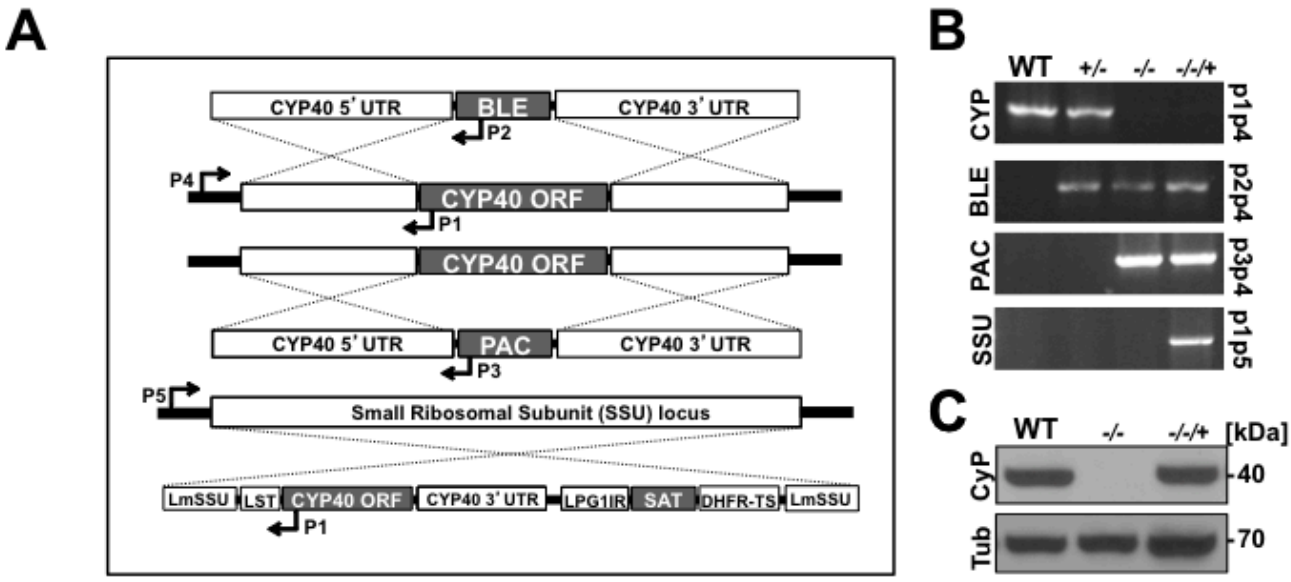
A
CYP40 5' UTR
BLE
CYP40 3' UTR
P2
P4
CYP40 ORF
P1
CYP40 ORF
CYP40 5' UTR
PAC
CYP40 3' UTR
P3
P5
Small Ribosomal Subunit (SSU) locus
LmSSU
LST
CYP40 ORF
CYP40 3' UTR
LPG1IR
SAT
DHFR-TS
LmSSU
P1
B
WT
+/-
-/-
-/-/+
CYP
p1p4
BLE
p2p4
PAC
p3p4
SSU
p1p5
C
WT
-/-
-/-/+
[kDa]
CyP
40
Tub
70

Figure 2

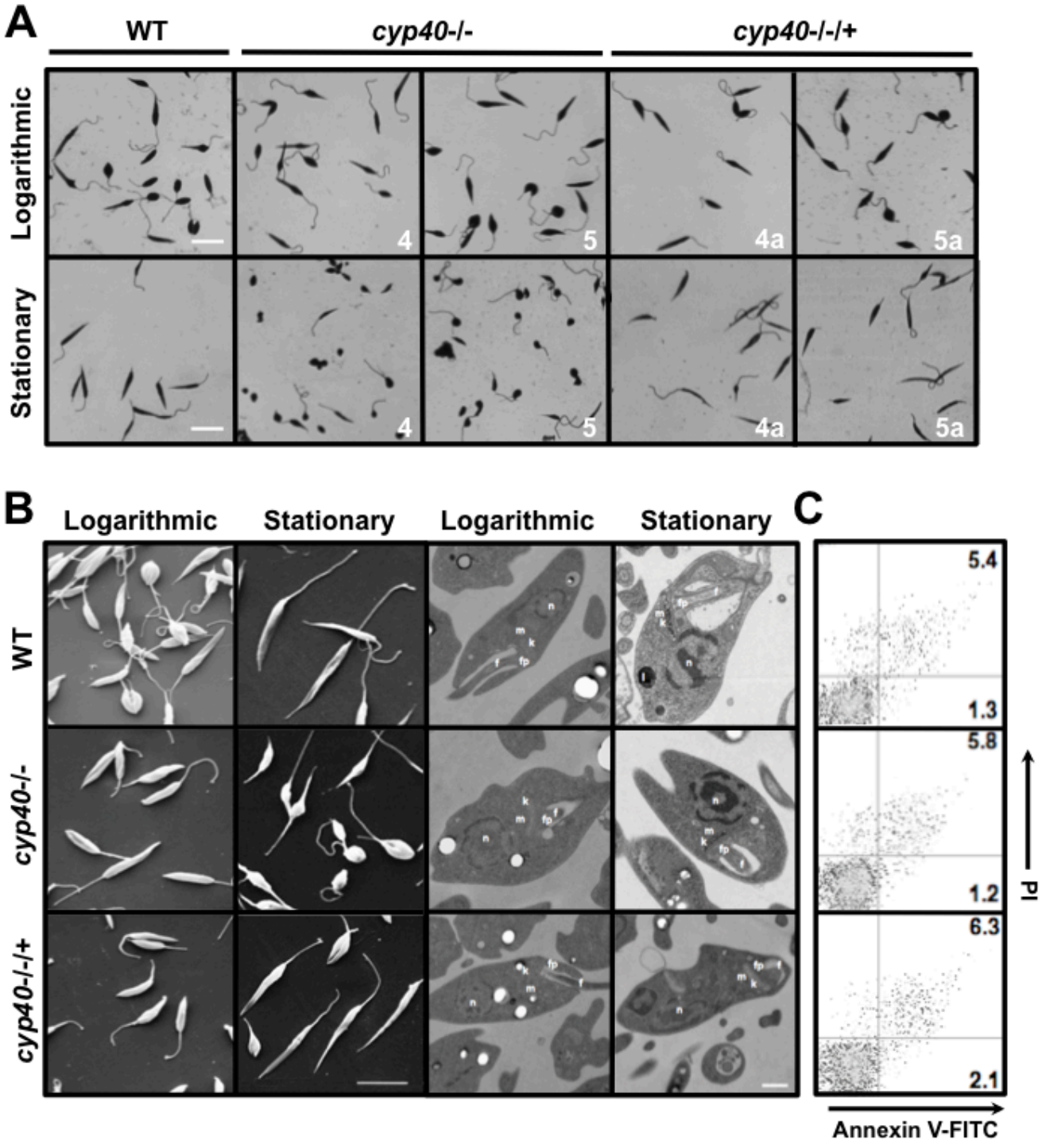
A
WT
cyp40-/-
cyp40-/-/+
Logarithmic
Stationary
4
5
4a
5a
B
Logarithmic
Stationary
Logarithmic
Stationary
WT
cyp40-/-
cyp40-/-/+
C
5.4
1.3
5.8
1.2
6.3
2.1
PI
Annexin V-FITC

Figure 3

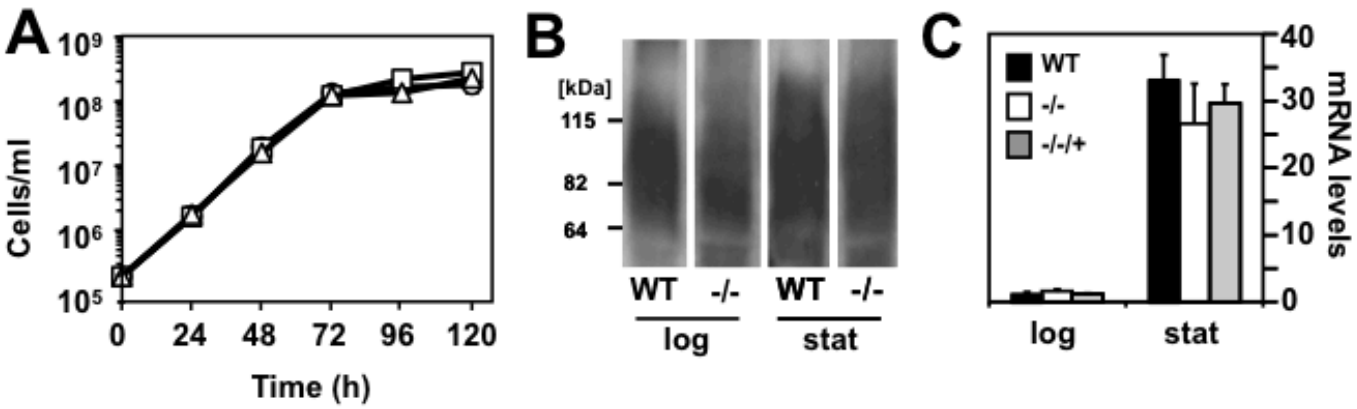
A
Cells/ml
10^9
10^8
10^7
10^6
10^5
0
24
48
72
96
120
Time (h)
B
[kDa]
115
82
64
WT
-/-
WT
-/-
log
stat
C
WT
-/-
-/-/+
40
30
20
10
0
mRNA levels
log
stat

Figure 4

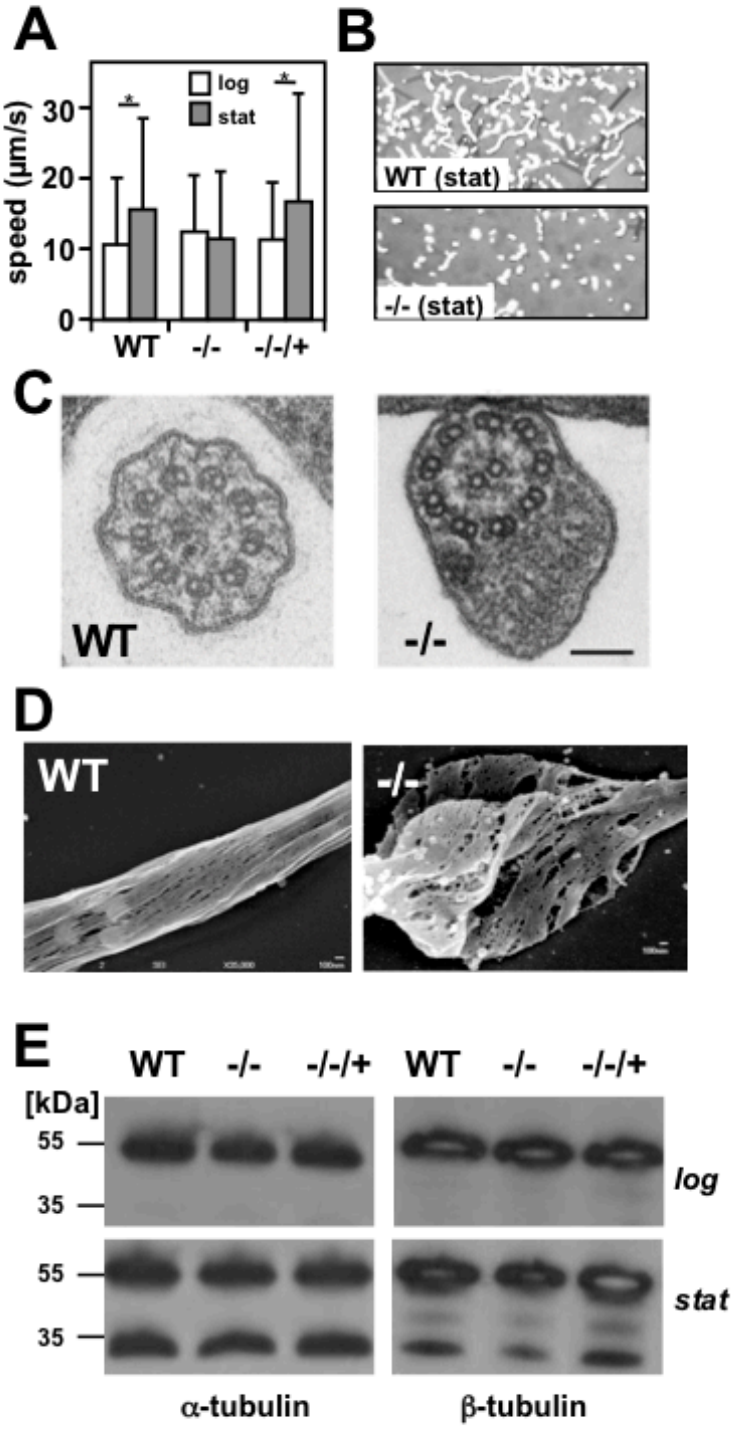
A
B
log
stat
speed (μm/s)
30
20
10
0
WT
-/-
-/-/+
WT (stat)
-/- (stat)
C
WT
-/-
D
WT
-/-
E
WT
-/-
-/-/+
WT
-/-
-/-/+
[kDa]
55
35
55
35
log
stat
α-tubulin
β-tubulin

Figure 5

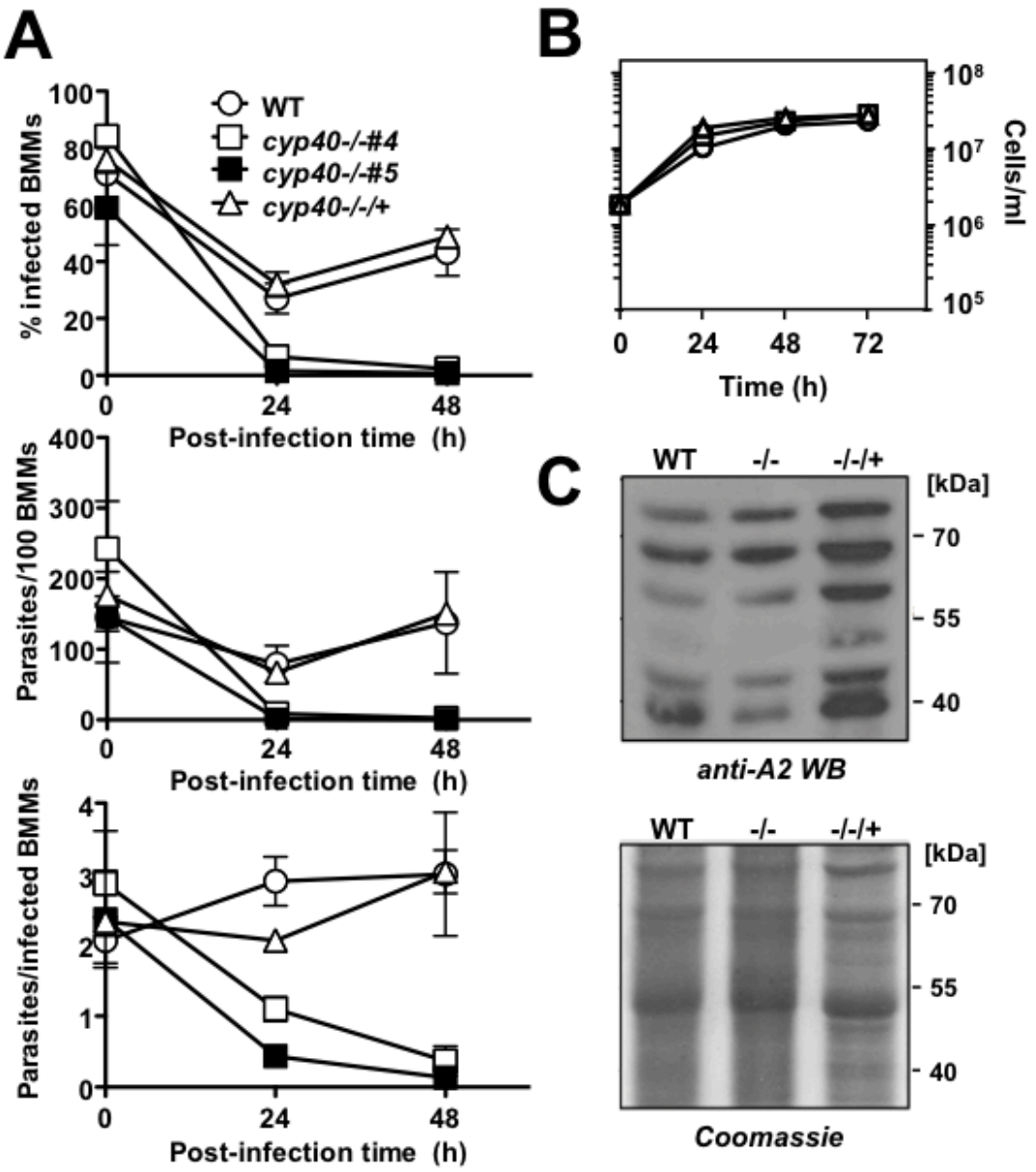
A
% infected BMMs
WT
cyp40-/-#4
cyp40-/-#5
cyp40-/-/+
Post-infection time (h)
Parasites/100 BMMs
Post-infection time (h)
Parasites/infected BMMs
Post-infection time (h)
B
Cells/ml
Time (h)
C
WT
-/-
-/-/+
[kDa]
anti-A2 WB
Coomassie

Figure 6

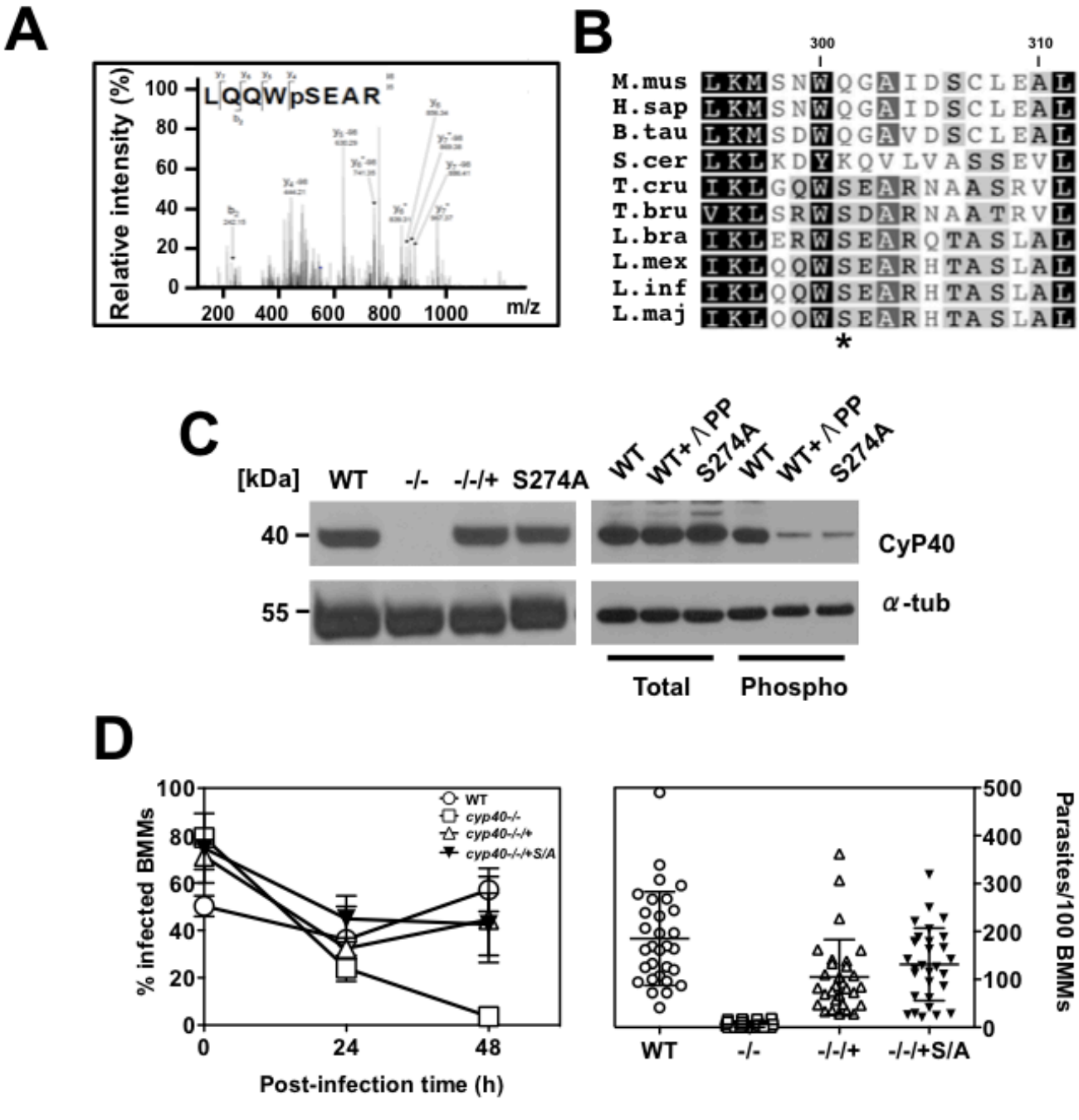
A
Relative intensity (%)
LQQWpSEAR
m/z
B
300
310
M.mus
H.sap
B.tau
S.cer
T.cru
T.bru
L.bra
L.mex
L.inf
L.maj
C
[kDa]
WT
-/-
-/-/+
S274A
WT+ΔPP
CyP40
α-tub
Total
Phospho
D
% infected BMMs
Post-infection time (h)
cyp40-/-
cyp40-/-/+
cyp40-/-/+S/A
Parasites/100 BMMs
-/-/+S/A

Figure 7

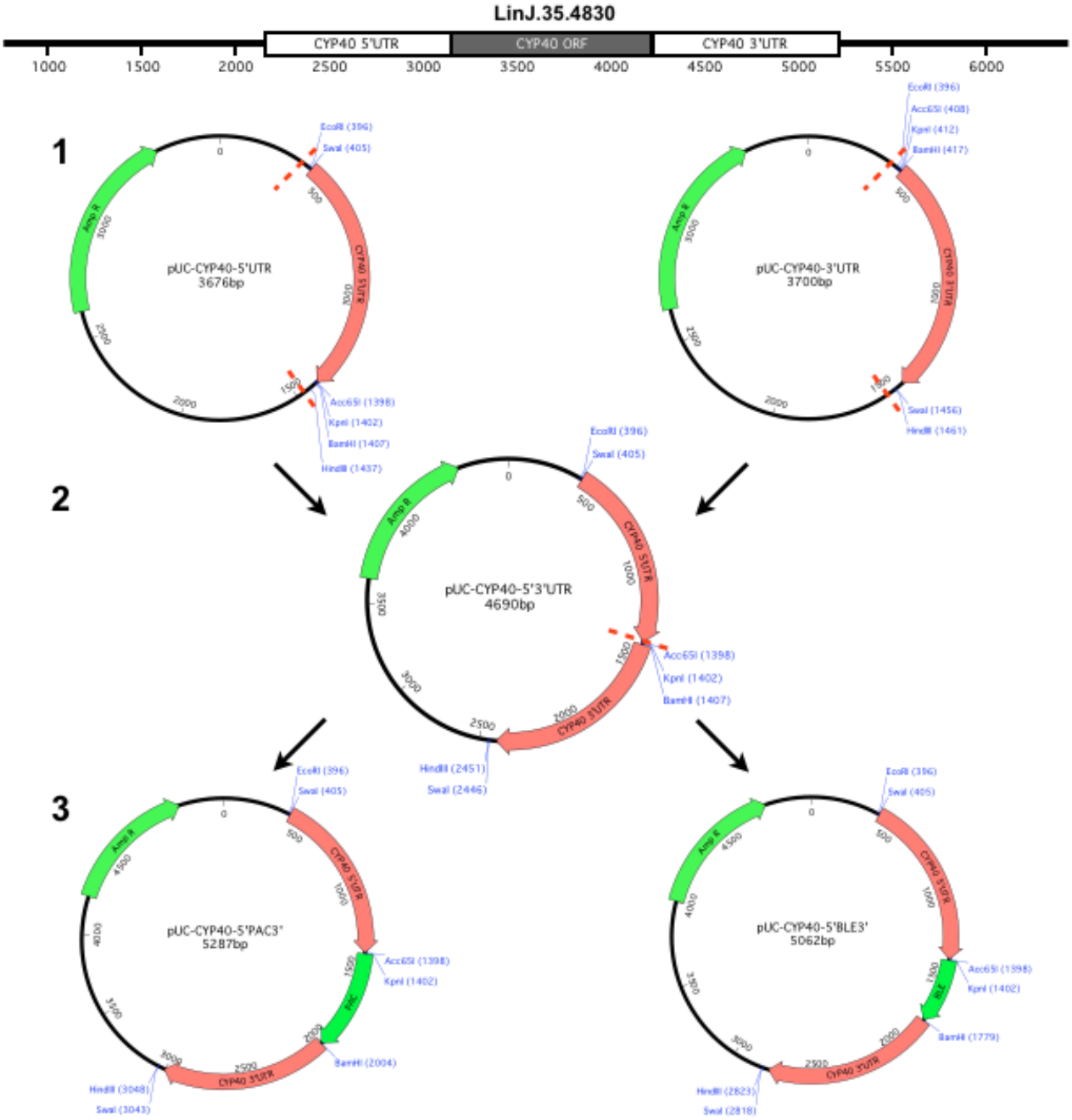
LinJ.35.4830
CYP40 5'UTR
CYP40 ORF
CYP40 3'UTR
1000
1500
2000
2500
3000
3500
4000
4500
5000
5500
6000
1
pUC-CYP40-5'UTR
3676bp
EcoRI (396)
SwaI (405)
Acc65I (1398)
KpnI (1402)
BamHI (1407)
HindIII (1437)
pUC-CYP40-3'UTR
3700bp
EcoRI (396)
Acc65I (408)
KpnI (412)
BamHI (417)
SwaI (1456)
HindIII (1461)
2
pUC-CYP40-5'3'UTR
4690bp
EcoRI (396)
SwaI (405)
Acc65I (1398)
KpnI (1402)
BamHI (1407)
HindIII (2451)
SwaI (2446)
3
pUC-CYP40-5'PAC3'
5287bp
EcoRI (396)
SwaI (405)
Acc65I (1398)
KpnI (1402)
BamHI (2004)
HindIII (3048)
SwaI (3043)
pUC-CYP40-5'BLE3'
5062bp
EcoRI (396)
SwaI (405)
Acc65I (1398)
KpnI (1402)
BamHI (1779)
HindIII (2823)
SwaI (2818)

Figure S1

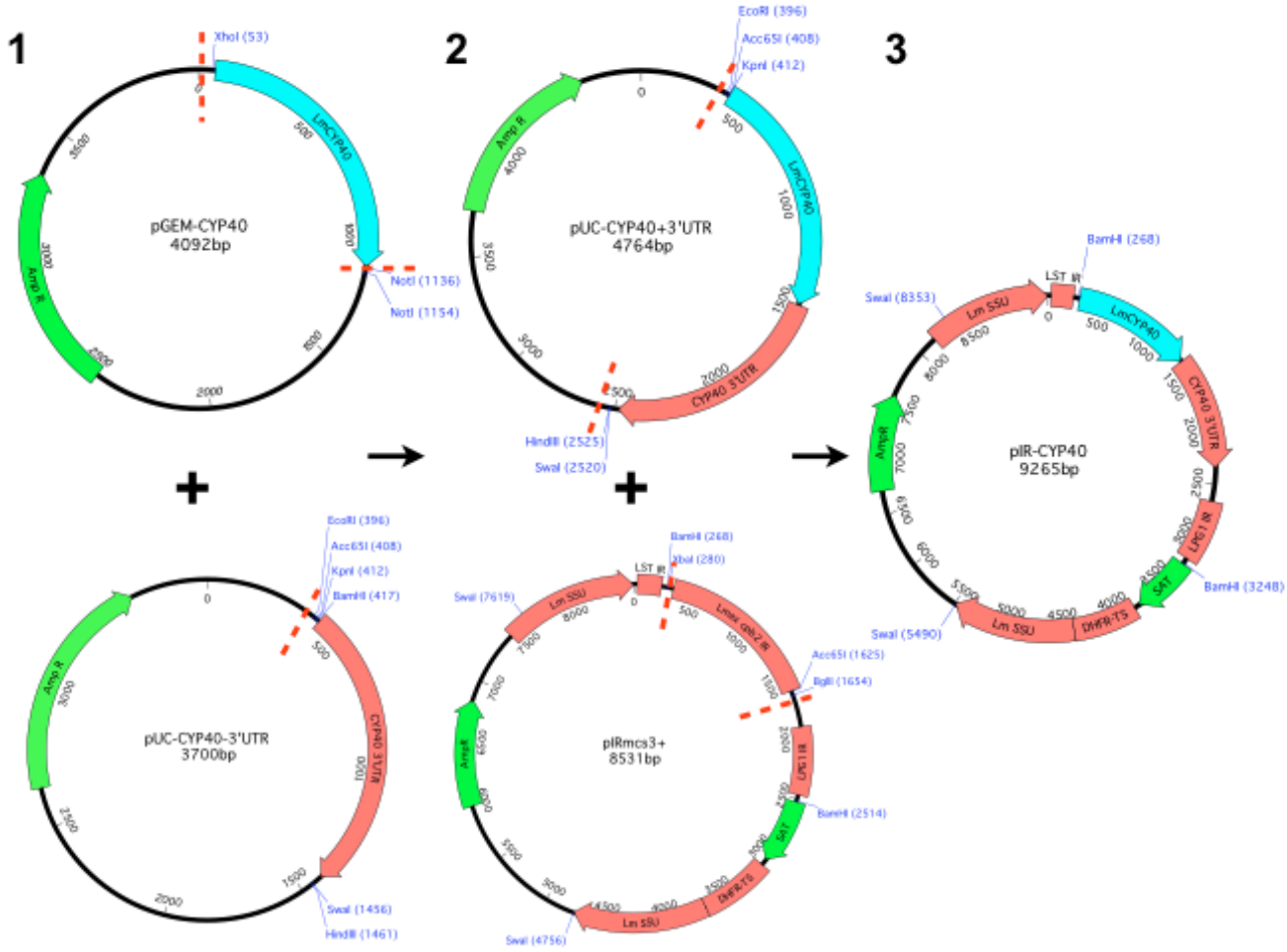
1
2
3
pGEM-CYP40
4092bp
XhoI (53)
NotI (1136)
NotI (1154)
LmCYP40
Amp R
pUC-CYP40+3'UTR
4764bp
EcoRI (396)
Acc65I (408)
KpnI (412)
HindIII (2525)
SwaI (2520)
CYP40 3'UTR
pUC-CYP40-3'UTR
3700bp
EcoRI (396)
Acc65I (408)
KpnI (412)
BamHI (417)
SwaI (1456)
HindIII (1461)
pIRmcs3+
8531bp
BamHI (268)
XhoI (280)
SwaI (7619)
SwaI (4756)
Acc65I (1625)
BglII (1654)
BamHI (2514)
LST IR
Lm SSU
Lmex cpb2.8
IR1
SAT
DHFR-TS
pIR-CYP40
9265bp
BamHI (268)
SwaI (8353)
SwaI (5490)
BamHI (3248)
AmpR

Figure S2

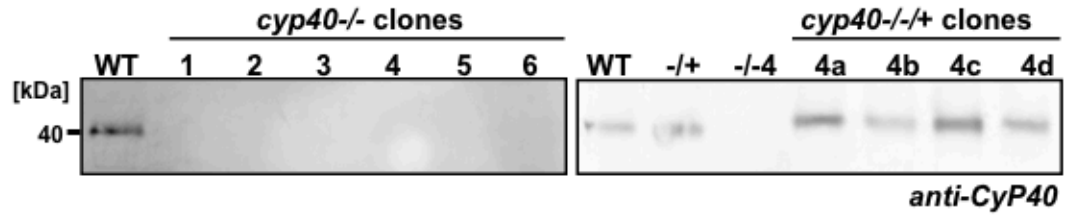
cyp40-/- clones
cyp40-/-/+ clones
WT
1
2
3
4
5
6
WT
-/+
-/-4
4a
4b
4c
4d
[kDa]
40
anti-CyP40

Figure S3

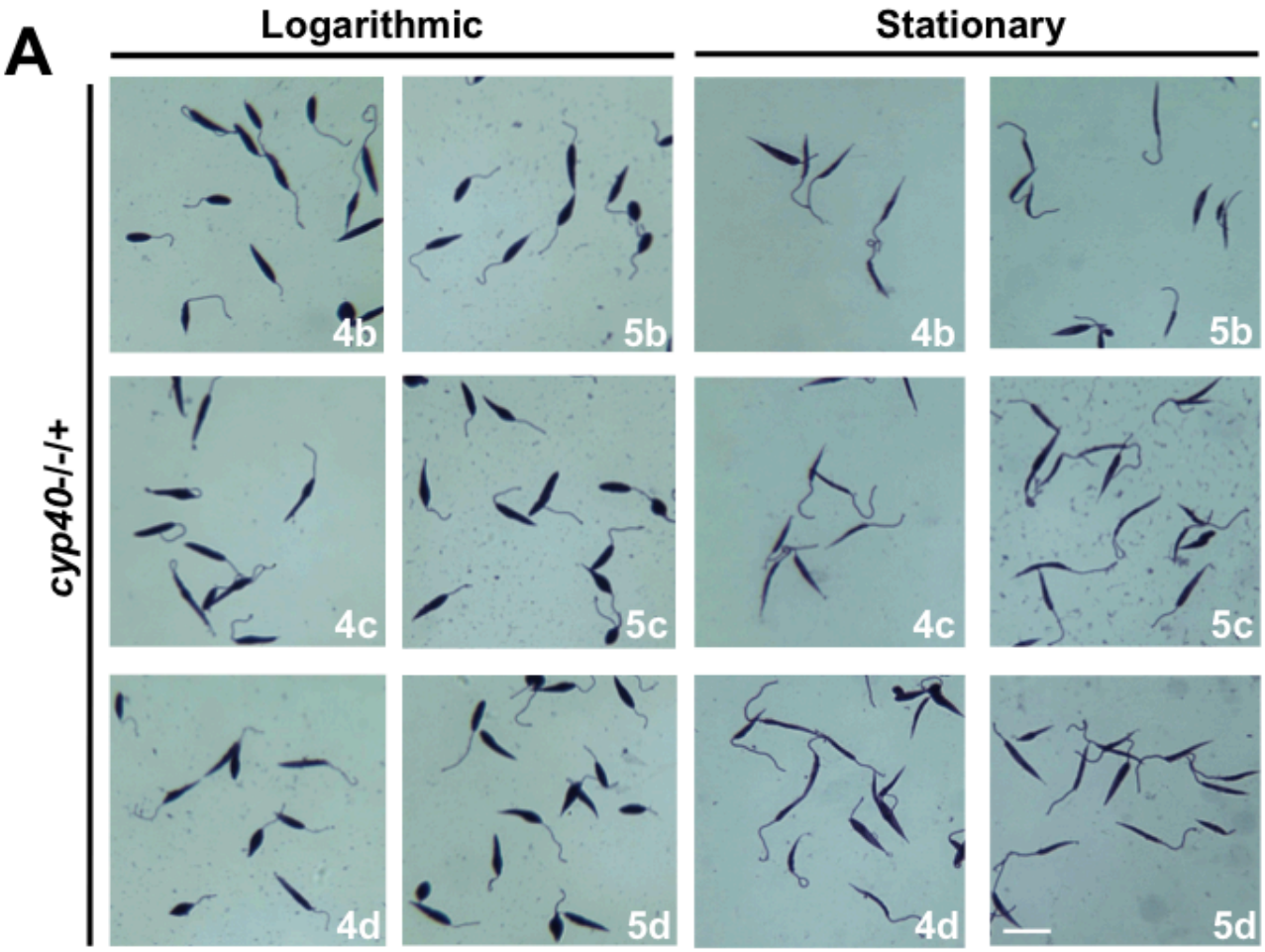
A
Logarithmic
Stationary
cyp40-/-/+
4b
5b
4b
5b
4c
5c
4c
5c
4d
5d
4d
5d

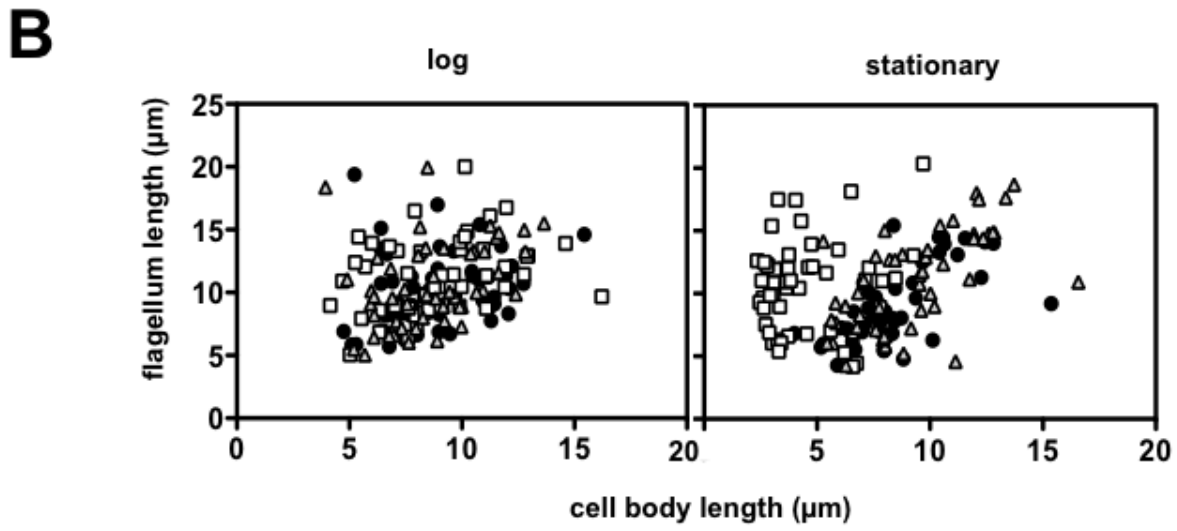
B
log
stationary
flagellum length (µm)
cell body length (µm)
0
5
10
15
20
25

Figure S4

A

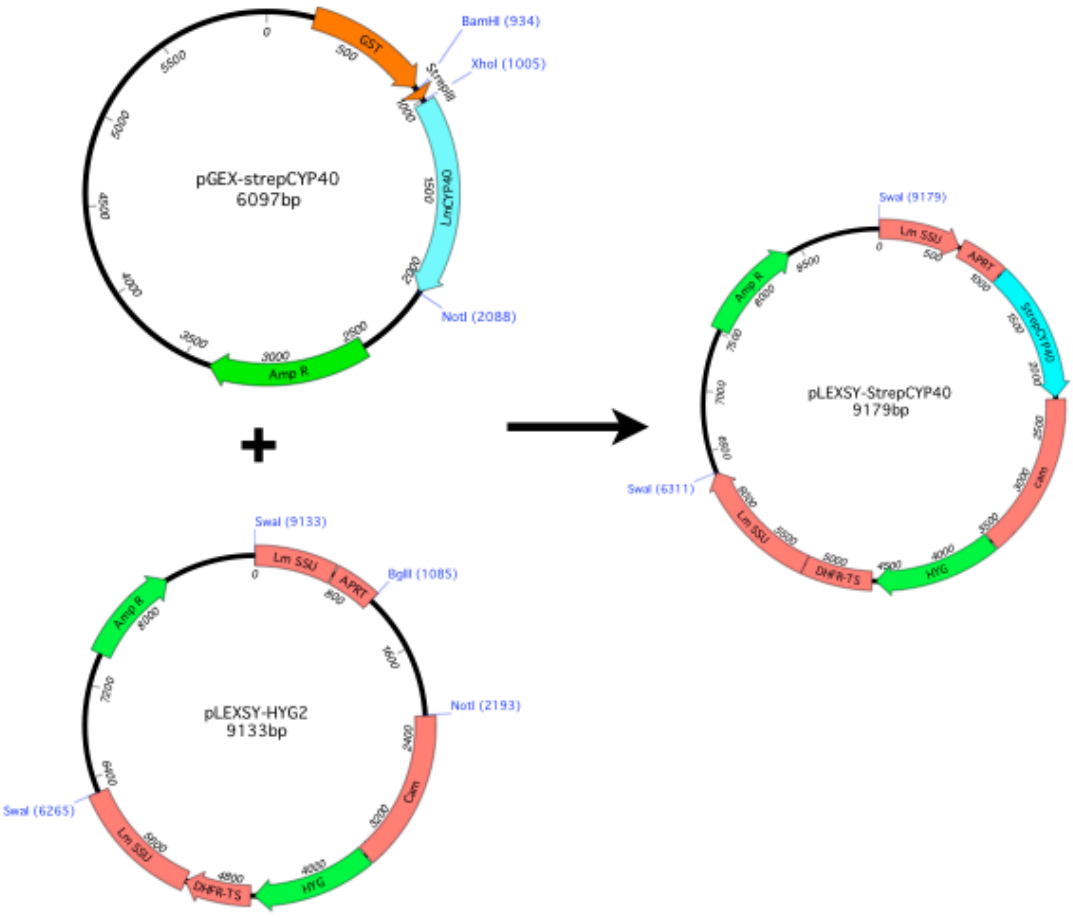
pGEX-strepCYP40
6097bp
GST
LmCYP40
Amp R
BamHI (934)
XhoI (1005)
StreptII
NotI (2088)
+
pLEXSY-HYG2
9133bp
SwaI (9133)
Lm SSU
APRT
BglII (1085)
NotI (2193)
Cam
HYG
DHFR-TS
SwaI (6265)
Amp R
pLEXSY-StrepCYP40
9179bp
SwaI (9179)
StrepCYP40
SwaI (6311)

B

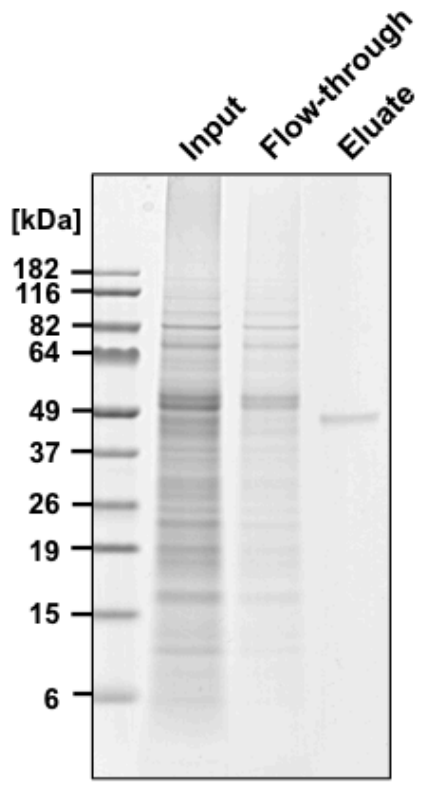
Input
Flow-through
Eluate
[kDa]
182
116
82
64
49
37
26
19
15
6

Figure S5

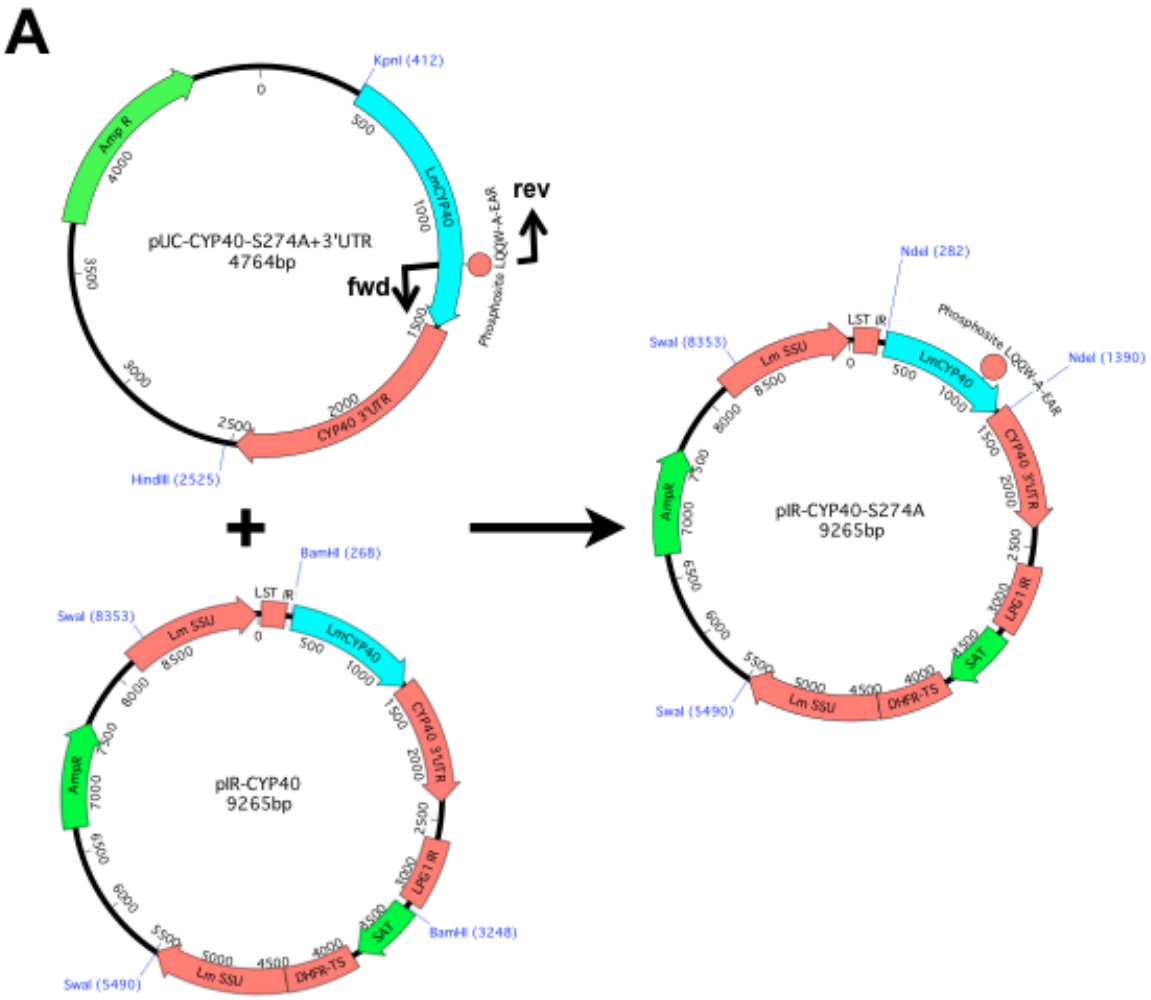
A
KpnI (412)
pUC-CYP40-S274A+3'UTR
4764bp
rev
fwd
HindIII (2525)
BamHI (268)
pIR-CYP40
9265bp
SwaI (5490)
NdeI (282)
NdeI (1390)
pIR-CYP40-S274A
9265bp
SwaI (5490)

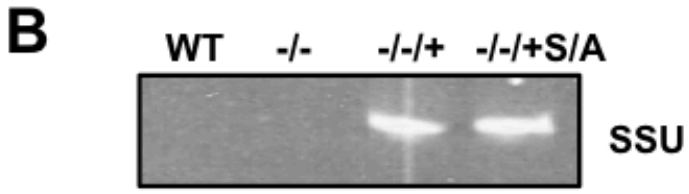
B
WT
-/-
-/-/+
-/-/+S/A
SSU

Figure S6

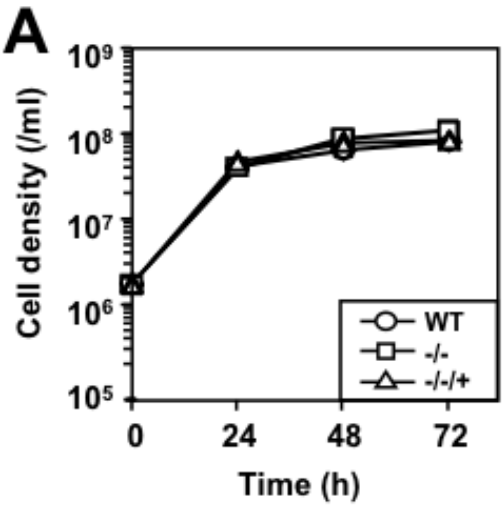
A
Cell density (/ml)
10^9
10^8
10^7
10^6
10^5
WT
-/-
-/-/+
0
24
48
72
Time (h)

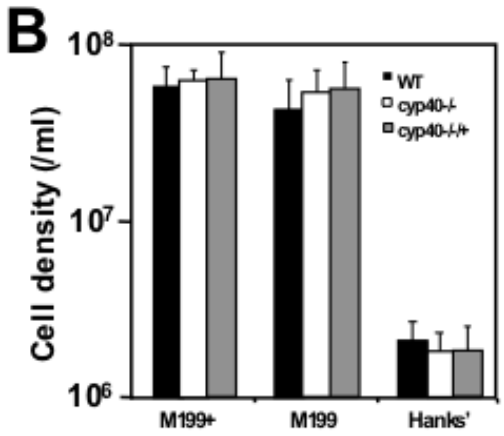
B
Cell density (/ml)
10^8
10^7
10^6
WT
cyp40-/-
cyp40-/-/+
M199+
M199
Hanks'

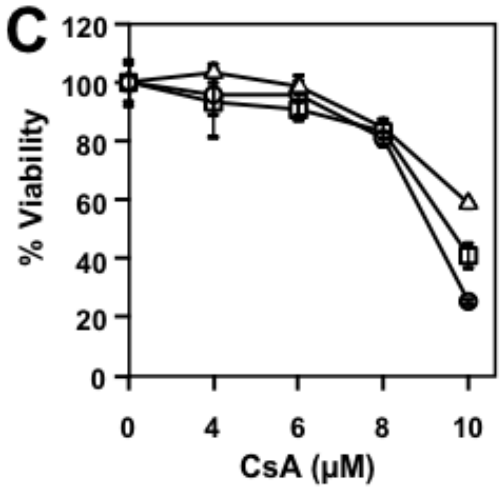
C
% Viability
120
100
80
60
40
20
0
0
4
6
8
10
CsA (μM)

Figure S7